The role of ion dissolution in metal and metal oxide surface inactivation of SARS-CoV-2

Jane Hilton[a*], Yoshiko Nanao[b*], Machiel Flokstra[b], Meisam Askari[b$], Terry K. Smith[a]
Andrea Di Falco[b] Phil D.C. King[b], Peter Wahl[b#], Catherine S Adamson[a#]

[a] Biomedical Sciences Research Complex, School of Biology, University of St Andrews, St Andrews, Fife, UK

[b] SUPA, School of Physics and Astronomy, University of St Andrews, St Andrews, Fife, UK

Running Head: Surface Inactivation of SARS-CoV-2

[#]Address correspondence to Catherine S Adamson, csa21@st-andrews.ac.uk or Peter Wahl, gpw2@st-andrews.ac.uk

* Jane Hilton and Yoshiko Nanao contributed equally to this work. Author order was determined as Jane Hilton contributed the biological data, presented in the paper, whereas Yoshiko Nanao generated the test surfaces used in the study.

[$] Present Address: Optek Systems, Abingdon, Oxford, UK

Abstract

Antiviral surface coatings are under development to prevent viral fomite transmission from high-traffic touch surfaces in public spaces. Copper's antiviral properties have been widely documented; but the antiviral mechanism of copper surfaces is not fully understood. We screened a series of metal and metal oxide surfaces for antiviral activity against severe acute respiratory syndrome coronavirus 2 (SARS-CoV-2), the causative agent of coronavirus disease (COVID-19). Copper and copper oxide surfaces exhibited superior anti-SARS-CoV-2 activity; however, level of antiviral activity was dependent upon the composition of the carrier solution used to deliver virus inoculum. We demonstrate that copper ions released into solution from test surfaces can mediate virus inactivation, indicating a copper ion dissolution-dependent antiviral mechanism. Level of antiviral activity is, however, not dependent on the amount of copper ions released into solution *per se*. Instead, our findings suggest that degree of virus inactivation is dependent upon copper ion complexation with other biomolecules (e.g., proteins/metabolites) in the virus carrier solution that compete with viral components. Although using tissue culture-derived virus inoculum is experimentally convenient to evaluate the antiviral activity of copper-derived test surfaces, we propose that the high organic content of tissue culture medium reduces the availability of "uncomplexed" copper ions to interact with the virus, negatively affecting virus inactivation and hence surface antiviral performance. We propose that laboratory antiviral surface testing should include virus delivered in a physiologically relevant carrier solution (saliva or

nasal secretions when testing respiratory viruses) to accurately predict real-life surface antiviral performance when deployed in public spaces.

Importance

The purpose of evaluating antiviral activity of test surfaces in the laboratory is to identify surfaces that will perform efficiently in preventing fomite transmission when deployed on high-traffic touch surfaces in public spaces. The conventional method in laboratory testing is to use tissue culture-derived virus inoculum, however this study demonstrates that antiviral performance of test copper-containing surfaces is dependent on the composition of the carrier solution in which the virus inoculum is delivered to test surfaces. Therefore, we recommend that laboratory surface testing should include virus delivered in a physiologically relevant carrier solution, to accurately predict real-life test surface performance in public spaces. Understanding the mechanism of virus inactivation is key to future rational design of improved antiviral surfaces. Here, we demonstrate that copper ions released from copper surfaces into small liquid droplets containing SARS-CoV-2, is a mechanism by which the virus that causes COVID-19 can be inactivated.

Introduction

Antiviral surface coatings are a non-pharmacological intervention that aim to prevent virus transmission via virus-contaminated surfaces, termed fomites (1). Fomite transmission occurs by hand contamination through touching fomites and subsequent self-inoculation by transfer of infectious virus from contaminated hands to exposed mucosal membranes in the mouth, nose, and eyes. Fomites are typically high-traffic touch surfaces, such as handles, push plates, lift buttons, railings, telephones, touch screens, counter tops etc., located in a wide range of public spaces. Particularly notable are ones located in healthcare settings such as hospitals and care homes. Fomite transmission plays an important role in the spread of enteric and respiratory viruses (2), although both groups of viruses have more than one route of transmission. Like other respiratory viruses, SARS-CoV-2, the causative agent of the COVID-19 pandemic, is primarily transmitted via droplet/aerosol mediated airborne transmission, but fomites are also considered a rare mode of SARS-CoV-2 transmission by the World Health Organisation (https://www.who.int/news-room/questions-and-answers/item/coronavirus-disease-covid-19-how-is-it-transmitted), the CDC (https://stacks.cdc.gov/view/cdc/104762) and others (3-5).

Fomite transmission requires that the virus remains viable on a surface long enough for onward human transfer. Laboratory studies have shown that high concentrations of SARS-CoV-2 remain viable on a timescale ranging from hours to days on a variety of commonly used surface materials such as stainless steel, plastic, and paper (5-7). Environmental studies have shown that SARS-CoV-2 RNA has been

detected on a wide range of surfaces in public spaces, particularly medical settings (4), however studies attempting to detect viable virus from such environmental surface usually fail to detect viable virus (8-10). Evidence that viable SARS-CoV-2 can be recovered from fomites in real-life settings is uncommon but has been reported (4, 11, 12). Longevity of viral surface survival is an important parameter affecting the likelihood of fomite transmission; prevention of fomite transmission depends on rapid inactivation of viruses on surfaces that act as fomites.

Surface survival times are dependent on the virus, the size of the initial inoculum, environmental factors (e.g., temperature, humidity) and surface properties (e.g., chemical composition, porosity) (2, 4). Development of surfaces with antiviral properties offers a long-term behaviour-independent strategy to prevent fomite transmission, as opposed to commonly employed short-term behaviour-dependent strategies including frequent hand washing and surface disinfection regimens. Copper and its alloys have long been known for their antimicrobial properties and laboratory studies of copper surfaces have been shown to inactivate a wide range of viruses, bacteria and fungi (13-15). The mechanism by which copper surfaces inactivate pathogens has not been fully elucidated, however with respect to viruses two key mechanisms have been proposed; (i) direct contact between the virus and the solid copper-containing surface (copper dissolution independent) and/or (ii) ion dissolution resulting in release of copper ions into solution from the copper-containing surface (copper dissolution dependent) (14). Virus inactivation has been reported to occur via damage to viral proteins, genomic material and envelopes (14).

In this study, we screened a series of metal and metal oxide surfaces for antiviral activity against SARS-CoV-2. Copper and copper oxide surfaces exhibited superior anti-SARS-CoV-2 activity; however, the level of antiviral activity was dependent upon composition of the carrier solution used to deliver virus inoculum. We demonstrate that copper ion dissolution is a mechanism of SARS-CoV-2 inactivation, but it is not dependent upon the amount of total copper ions released into solution per se. Instead, we suggest that the degree of virus inactivation is dependent upon copper ion complexation with other biomolecules in the virus inoculum that compete with viral components. Based on our findings, we recommend that laboratory antiviral surface testing should include virus delivered in a physiologically relevant carrier solution (i.e., saliva or nasal secretions when testing respiratory viruses) to predict real-life test surface performance more accurately when deployed in public spaces.

Results

SARS-CoV-2 is inactivated upon exposure to copper surfaces.

The antiviral properties of copper are confirmed against SARS-CoV-2, by its time dependent inactivation upon exposure to bulk copper foil or thin-film evaporated copper test coupons (Fig. 1). Significantly less virus inactivation occurred upon exposure to stainless steel and the virus remains consistently viable across the time series with respect to the no coupon control. SARS-CoV-2 inactivation was essentially comparable between the two types of copper samples studied. No viable virus was detectable after 120-min exposure to either copper surface, demonstrating that exposure to a copper

surface requires at least 1-2 hours to efficiently inactivate the virus inoculum used (~ 4,000 PFU/7 μL in Dulbecco's Modified Eagle's Medium supplemented in 2% v/v FBS (DMEM-2%FBS)). We applied an exponential fit to our data to determine the mean half-life of the virus when exposed to copper surfaces (Fig. 1B), which was 38 and 28 minutes for the copper foil and evaporated copper surfaces respectively. Therefore, a 30-min exposure to a copper surface results in ~50% virus inactivation (Fig. 1A), providing an ideal time point to screen further test coupons to identify surface materials that inactivate SARS-CoV-2 faster than copper and thus demonstrate improved antiviral properties.

Screening metal and metal oxide surfaces revealed that Cu_2O containing surfaces exhibited SARS-CoV-2 antiviral activity superior to elemental copper.

Utilizing the 30-min copper exposure time point as a screening reference point, a selection of different surfaces were tested with the aim of identifying materials that exhibit antiviral activity superior to copper. The thin-film evaporated copper coupon (500 nm thickness) was chosen as the standard reference point (referred to as copper), along with stainless steel and no coupon controls, for screening purposes and throughout the manuscript. Screening was performed using the same SARS-CoV-2 inoculum described above (~ 4,000 PFU/7 μL in DMEM-2%FBS).

Initially, we generated a series of coupons with elemental metal surfaces; transition metals silver (Ag), nickel (Ni) and palladium (Pd) were selected based on their proximity to copper in the periodic table, along with post-transition metal bismuth (Bi) (Table S1 and S2). Upon exposure of SARS-CoV-2 to the test elemental metal surfaces

158 it was clearly apparent that copper exhibited the best antiviral activity (Fig. 2A). We next
159 investigated the antiviral properties of transition metal oxide surfaces. In the first
160 instance, we generated delafossite copper chromate ($CuCrO_2$), titanium oxide (TiO_2)
161 and indium tin oxide (ITO) films (Table S1 and S2). ITO was particularly selected as a
162 transparent conductor, with widespread applications in touch screen surfaces.
163 Unfortunately, these test surfaces did not result in any substantial SARS-CoV-2
164 inactivation and again copper exhibited the best antiviral activity (Fig. 2B).

165 Given that copper consistently exhibited the best antiviral activity, we proceeded
166 to test copper oxide surfaces. Using two different methods, we generated two types of
167 copper oxide surfaces: (i) an annealed mixture of cupric oxide and cuprous oxide
168 (CuO/Cu_2O), and (ii) a copper oxide thin film consisting predominantly of cuprous oxide
169 (Cu_2O) (Table S1 and Fig.S1). Each type of copper oxide surface was generated at two
170 different thicknesses (Table S1). The copper oxide surfaces all exhibited significant
171 antiviral activity (Fig. 2C). Importantly, the Cu_2O thin-film exhibited better virus
172 inactivation than annealed copper surfaces containing a CuO/Cu_2O mixture in the
173 surface layer, suggesting that the Cu_2O oxidation state has superior antiviral properties.
174 Most notably, the Cu_2O thin-films resulted in better virus inactivation than the copper
175 reference coupon, with the thicker (~30 nm) Cu_2O film resulting in ~75% SARS-CoV-2
176 inactivation after 30 min exposure, which represents an improvement of inactivation by
177 ~50% compared to copper. For the mixed CuO/Cu_2O samples, we found that the more
178 oxygen-rich CuO phase forms as the surface layer, with Cu_2O forming below the
179 surface (Fig. S2), inhibiting the superior antiviral properties of Cu_2O. Interestingly, we
180 also observed increased antiviral activity for the thicker (~30 nm) copper oxide films,

with a somewhat reduced inactivation for the ultrathin (~10 nm) film thickness. Overall, we show that thin films exposing Cu_2O at the surface have superior antiviral properties over an evaporated and post-oxidized copper surface and that for films with a thickness of tens of nanometers, the film thickness can limit the degree of antiviral activity observed.

Increasing copper surface thickness correlates with increased SARS-CoV-2 inactivation. Motivated by these findings of a thickness-dependent antiviral activity of copper oxide films, we took advantage of our ability to precisely control film thickness by generating a series of evaporated copper films with thicknesses of 5, 10, 20, 50, 100, 250 and 500 nm. In agreement with our previous observations, the amount of SARS-CoV-2 inactivation after 30-min exposure increased stepwise with film thickness from 5-50 nm and stabilized at ~50% inactivation when exposed to copper films of ≥50 nm (Fig. 3A). The stabilization at ≥50 nm is likely to be a function of the 30-min copper exposure time, as we demonstrated in Fig. 1A, where further inactivation occurs after 60- and 120-min exposure to a 500 nm copper film. We also observed that following removal of 7 μL in DMEM-2%FBS after 30-min exposure time, the copper film appeared modified on the coupons generated with a copper film thickness of 50 nm, whereas the copper film remained visible on coupons with a 500 nm layer (Fig. 3B). These observations, combined with the fact that increasing copper film thickness correlates with increased SARS-CoV-2 inactivation, suggests that dissolution of copper ions into solution might be the mechanism driving virus inactivation.

Different carrier solutions impact SARS-CoV-2 inactivation, but inactivation does not correlate with amount of Cu ions released into solution.

Understanding the mechanism of virus inactivation is key to future rational design of improved antiviral surfaces. Although the antiviral mechanism remains poorly understood two main hypotheses have been proposed; (i) direct contact between the virus and the solid copper-containing surface (copper dissolution independent) and/or (ii) ion dissolution resulting in release of copper ions into solution from the copper-containing surface (copper dissolution dependent) (14). To further investigate the role of copper ion dissolution we hypothesized that if the virus was delivered to a test copper surface in carrier solutions that differentially dissolve copper ions, then virus inactivation would be correspondingly affected. We selected the following carrier solutions; DMEM-2%FBS, phosphate buffered saline (PBS) and artificial saliva (AS). DMEM-2%FBS is equivalent to the virus inoculum used in our prior experiments, PBS is a physiological buffered solution commonly used in cell culture and AS was selected to simulate a real-world scenario related to transmission of respiratory viruses such as SARS-CoV-2.

ICP-OES (Inductively Coupled Plasma - Optical Emission Spectroscopy) was used to determine Cu ion concentration released into 7 μL of each carrier solution following a 30-min exposure to either reference evaporated copper (500 nm) or Cu_2O (30 nm) containing thin-film coupons (Fig. 4A). The largest amount of Cu ion dissolution was observed upon DMEM-2%FBS exposure to evaporated copper followed by Cu_2O containing coupons. Approximately one third the level of copper ions was released upon PBS exposure for both coupon types and the least amount was observed upon AS

exposure, which resulted in a low-level ion release from the Cu_2O coupon and no detectable release of copper ions for the evaporated copper coupon.

We next tested virus inactivation following exposure to evaporated copper coupons when SARS-CoV-2 is delivered as an inoculum of ~4,000 PFU in 7 μL of each carrier solution. Importantly, we confirmed that SARS-CoV-2 remained comparably viable in each carrier solution; this was tested by measuring SARS-CoV-2 titre after resuspension in each carrier solution to confirm equal virus input (Fig. S3) and is demonstrated by the virus remaining consistently viable across the time series for each carrier solution with respect to the no coupon control (Fig. 4B-D). At the previously used 30-min exposure time, SARS-CoV-2 in DMEM-2%FBS resulted in ~70% inactivation, unexpectedly however viable virus was undetectable when SARS-CoV-2 was delivered in either PBS or AS (Fig. 4B). On the 3rd and final repeat of this experiment we conducted coupon exposure at reduced time points of 20- and 10-mins, reassuringly the level of SARS-CoV-2 inactivation was time dependent for each carrier solution (Fig. 4C and D). Overall, we show that virus inactivation is impacted by virus carrier solution and the most effective inactivation occurred when virus was delivered in PBS. However, the level of SARS-CoV-2 inactivation does not appear to correlate with the amount of available copper ions in the presence of the different virus carrier solutions.

Copper ion dissolution and availability is a mechanism that can independently lead to SARS-CoV-2 inactivation. To directly test the role of copper ion dissolution in SARS-CoV-2 inactivation, we performed a variation of the test surface inactivation assay, in which virus inactivation is de-coupled from the test copper surface. First, 7 μL

of each carrier solution was added to either evaporated copper or Cu_2O containing thin-film coupons and incubated for 0- or 30-mins. The carrier solution (together with any released copper ions) was then removed from the test surface and spiked with 2 μL SARS-CoV-2 inoculum containing ~4,000 PFU and further incubated for 0- or 30-mins. To act as a control, we performed a test surface inactivation assay (Fig. 5A and B) in parallel to the de-coupled assay (Fig. 5C and D).

As expected from the result shown in Fig. 2C, 30-min exposure of SARS-CoV-2 in DMEM-2%FBS to either an evaporated copper or Cu_2O coupon resulted in ~50% and ~90% inactivation respectively (Fig. 5A and B). In agreement with the results described in Fig. 4B, 30-min exposure of SARS-CoV-2 in PBS or AS to an evaporated copper coupon resulted in 100% inactivation (Fig. 5A). However, upon exposure to a Cu_2O surface SARS-CoV-2 in AS only resulted in 50% inactivation (Fig. 5B), thus the presence of the Cu_2O did not result in the improved virus inactivation observed when virus is delivered in DMEM-2%FBS. In fact, superior inactivation occurred when SARS-CoV-2 is delivered in AS and exposed to the evaporated copper surface (Fig. 5A and B).

The de-coupled assay, which directly tests if copper ions released into solution can inactivate virus, showed that the DMEM-2%FBS-based solution recovered from either evaporated copper or Cu_2O containing surfaces was not capable of any SARS-CoV-2 inactivation (Fig. 5C and D), despite the ICP-OES analysis demonstrating that the greatest level of copper ions is released when coupons are exposed to DMEM-2%FBS (Fig. 4A). In contrast, the PBS-based solution recovered from either surface was capable of ~50% virus inactivation (Fig. 5C and D) providing evidence that copper

ion dissolution, and hence Cu ion released into solution, can be a mechanism directly and independently responsible for virus inactivation, but no advantage was afforded by release of ions from the Cu_2O film. Curiously, the AS-based solution recovered from the evaporated copper surface was not capable of virus inactivation (Fig. 5C), yet the AS-based solution recovered from the Cu_2O containing surface resulted in the most potent virus inactivation (~80%) observed for the de-coupled assay and surprisingly was even better than the level of inactivation when virus in AS was in direct contact with the Cu_2O containing surface (Fig. 5D). Overall, we show that copper ions resulting from dissolution independent of the direct surface contact is a mechanism that can independently lead to SARS-CoV-2 inactivation, but this mechanism is influenced by the properties of the carrier solution and the type of copper ions.

Discussion

Copper has been widely documented to exert antiviral activity however, the mechanism of action is not fully understood. In this study we further investigate the role of ion dissolution as a mechanism by which copper and copper oxide surfaces inactivate SARS-CoV-2. First, we confirmed that SARS-CoV-2 is efficiently inactivated upon exposure to copper surfaces, in broad agreement with other SARS-CoV-2 studies (6, 16-20).

We screened a series of metal coupons with the aim of identifying a surface that inactivates SARS-CoV-2 faster than copper. Despite antimicrobial properties of silver being widely reported (21), we show that a silver surface did not exhibit extensive

SARS-CoV-2 inactivation. Others have also reported silver materials to lack antiviral activity against SARS-CoV-2 and other viruses (16, 18, 22, 23) and the poor antiviral activity has been proposed to be due to low levels of Ag ion dissolution (16, 22). In contrast, positive reports of silver antiviral activity generally relate to silver-containing nanoparticles (24-28). The other elemental metals tested in this study (nickel, palladium and bismuth) also exhibited weak antiviral activity against SARS-CoV-2.

We tested a series of transition metal oxide surfaces. A titanium oxide (TiO_2) surface did not result in a substantial level of SARS-CoV-2 inactivation. TiO_2 has photocatalytic properties that following light illumination generates highly oxidizing free radicals (reactive oxygen species) that are reported to have antibacterial and antiviral activity (29). Our experimental procedure did not include a deliberate illumination step; however, it has been reported that when illumination of TiO_2 or TiO_2-composite surface coatings is undertaken, significant levels of SARS-CoV-2 inactivation occur (30-34). Weak anti-SARS-CoV-2 activity was observed upon exposure to an indium tin oxide (ITO) surface, which was tested due to its transparent properties in thin layers that could be applied to touchscreen surfaces. Whilst our study was ongoing, others reported different strategies that generated transparent surface coatings which exhibited significant anti-SARS-CoV-2 activity (35-37).

In addition to copper, we show that copper oxide (Cu_2O-containing) test surfaces exhibited significant anti-SARS-CoV-2 activity, in agreement with other studies that have reported various copper oxide surfaces (CuO and/or Cu_2O) to exhibit effective anti-SARS-CoV-2 activity (37-41). Importantly however, we demonstrate that the level of antiviral activity was strikingly dependent on the composition of carrier solution in which

318 the virus inoculum was delivered to test surfaces. From our data, it can be concluded
319 that when SARS-CoV-2 is delivered in DMEM-2%FBS (tissue culture media) a copper
320 oxide surface (with Cu_2O as the predominant oxidation phase) resulted in significantly
321 better virus inactivation than the reference copper surface. However, the reverse is
322 concluded when SARS-CoV-2 is delivered in AS (artificial saliva), as the reference
323 copper surface exhibited superior antiviral activity over the Cu_2O-containing surface.
324 Further, SARS-CoV-2 delivered in PBS (phosphate buffered solution) resulted in the
325 best virus inactivation whichever copper or Cu_2O-containing surface was tested.

326 The purpose of evaluating antiviral activity of test surfaces in the laboratory is to
327 identify surfaces that will perform efficiently in preventing fomite transmission when
328 deployed on surfaces in public spaces. Therefore, although it is experimentally
329 convenient to use a tissue culture derived virus inoculum (typically DMEM or MEM with
330 various FBS concentrations up to 10%) for evaluating the antiviral properties of test
331 surfaces in the laboratory (6, 16-20, 37-41), we clearly demonstrate that antiviral
332 performance of test surfaces is dependent upon the composition of the virus carrier
333 solution. In real life, SARS-CoV-2 is expelled from an infected person via respiratory
334 (saliva/sputum) droplets/aerosols, the composition of which is not accurately
335 represented by tissue culture medium supplemented with FBS. In this study, we tested
336 an artificial saliva carrier solution (42) formulated to mimic human saliva, which is a very
337 dilute fluid composed of >97% water plus electrolytes, proteins/enzymes (43). Overall,
338 our results suggest that future studies would ideally include virus delivered in
339 physiologically relevant carrier solution, e.g., real human saliva/sputum samples when

testing respiratory viruses, to recapitulate a real-life scenario to obtain a more realistic determination of test surface antiviral performance.

We hypothesized that composition of virus carrier solution could influence copper ion dissolution from copper/copper oxide surfaces, which would in turn effect surface antiviral performance if copper ion dissolution plays an important mechanistic role in antiviral activity. Indeed, we demonstrate that the different carrier solutions used in this study do influence the amount of copper ions released into solution from copper and Cu_2O-containing surfaces, with the largest amount of copper ions released upon surface exposure to DMEM-2%FBS (tissue culture medium). In agreement with our observations, others have also reported that different liquids vary the level of ion release from copper and copper oxide surfaces and that the highest levels of release are into liquids containing amino acids, proteins or complex organic materials (44-47). Some studies have reported a positive correlation between the amount of copper ion released from copper/copper surfaces and antibacterial activity (47, 48). However, we did not observe any correlation between SARS-CoV-2 inactivation and total amount of copper ions released in the presence of the different virus carrier solutions used in this study. Nevertheless, we proceeded to further investigate the role of copper ion dissolution, as our observation that surface thickness influenced level of antiviral activity also suggests that ion dissolution may play a mechanistic role in antiviral activity.

To do this, we performed a variation of the test surface inactivation assay, in which virus inactivation is de-coupled from the test copper/copper oxide surface to directly test if copper ions released into solution are capable of virus inactivation. Our results show that copper ions released into DMEM-2%FBS solution following copper or

Cu_2O-containing surface exposure, did not have the capacity to inactivate SARS-CoV-2. A reasonable interpretation of this observation could be that ion dissolution does not play a significant role in virus inactivation and instead direct surface contact killing is the major mechanism of action at play. Indeed, Hosseini *et al*., used a similar experimental approach to determine the role of copper ions released from a cupric oxide (CuO) film exposed to virus culture medium; material leached from their CuO coating did not inactivate SARS-CoV-2 and thus they rejected the hypothesis that dissolved material was the cause of inactivation and concluded that direct contact between SARS-CoV-2 and CuO is necessary to inhibit infection (38). Importantly, an alternative interpretation is required to explain our observations, because we provide direct evidence that copper ion dissolution is a mechanism by which SARS-CoV-2 can be inactivated, as material released into PBS solution following copper or Cu_2O-containing surface exposure exhibited significant antiviral activity. The inactivation rate attributed to copper ion dissolution was ~50% less than that observed when an equivalent virus inoculum was directly exposed to test surfaces, indicating that copper ion dissolution is not the only antiviral mechanism, and that direct contact killing may also play a role.

The question remains if copper ions released from our test surfaces are innately capable of virus inactivation, why doesn't SARS-CoV-2 inactivation occur in DMEM-2%FBS solution released from our test surfaces? We propose that copper complexation with biomolecules (e.g., proteins, metabolites) in DMEM-2%FBS reduces the bioavailability of copper ions, therefore when SARS-CoV-2 is retrospectively added to released DMEM-2%FBS solution the copper ions are no longer available to interact with SARS-CoV-2 and thus virus inactivation does not occur. In support of this, Hedberg *et*

386 *al*., demonstrated that copper ions released from Cu nanoparticles in biomolecule-
387 containing media (e.g., DMEM, DMEM supplemented with FBS, or PBS supplemented
388 with the amino acid histidine) does not exist as free Cu^{2+} ions in solution, but was
389 instead completely complexed via strong bonds to biomolecules, conversely copper
390 ions released from Cu nanoparticles in PBS formed labile Cu-complexes (44).
391 Therefore, our interpretation of the data does not reject copper ion dissolution as an
392 antiviral mechanism, on the contrary we provide direct evidence in support of copper ion
393 dissolution as a mechanism that contributes to the antiviral activity of copper/copper
394 oxide surfaces. Further, we suggest that complexation of dissolved copper ions with
395 biomolecules present in the virus carrier solution can influence surface antiviral
396 performance. We envision that competition between biomolecules in the carrier solution
397 and the surface of SARS-CoV-2 for copper ion complexation could explain why our
398 copper surfaces perform better when virus inoculum is delivered in PBS (which forms
399 liable weak copper complexes) compared to DMEM-2%FBS (which forms strong
400 chelating complexes) and further would explain why we did not observe a clear positive
401 correlation between level of copper ion release into solution and antiviral activity. In
402 support, whilst our manuscript was being prepared Glover *et al*., reported that
403 coronavirus (OC43) inactivation on copper surfaces is significantly faster when virus
404 was delivered in artificial perspiration solution compared to assay medium (DMEM) (46).
405 Like our data, the rate of virus inactivation did not correlate with total amount of copper
406 ions released into solution, instead they also suggest that chelated copper cations are
407 not available for virus inactivation and that the organic constituents of DMEM act as
408 chelators. Also, Sharan *et al*., who studied inactivation of *E.coli* suspensions in copper

409 water storage vessels concluded that addition of amino acids, proteins or complex
410 organic mixtures caused a dramatic decrease in *E.coli* inactivation, likely as a
411 consequence of complex formation between leached copper and the organic
412 constituents (45). Behzadinasab *et al*., examined the effect of dissolved copper ion
413 species (leachate) from Cu_2O microparticles suspended in different solutions (including
414 PBS and DMEM-2%FBS) on killing of gram-negative bacterium *Pseudomonas*
415 *aeruginosa* (47). In agreement with our observations, concentration of dissolved copper
416 species was dependent on solution composition with the largest concentration of copper
417 leached into DMEM-2%FBS. However, in direct contrast to our observation with SARS-
418 CoV-2, killing of *P. aeruginosa* correlated with dissolved copper ion concentration;
419 copper leached into PBS did not kill the bacterium yet DMEM-lechate killed >99.9%,
420 with solubilized Cu^+ reported to be the potent active antimicrobial species. Under their
421 experimental conditions copper's antimicrobial activity against P. *aeruginosa* occurred
422 via an ion dissolution dependent mechanism and direct contact was not required for
423 killing, although proximity to the source of copper ions is important. In-step with our
424 conclusions, it is noted that "their observations are important because a variety of media
425 (buffers) is used in antimicrobial testing, and those media are not always the same as
426 the bodily fluid that carries the microbes or viruses".

427 A further consequence of proteins in virus carrier solutions, that should be
428 considered, is that their presence has been shown to confer a protective effect that
429 stabilizes enveloped viruses (including SARS-CoV-2) over time, prolonging virus
430 surface viability and hence delaying the rate of environmental decay (7, 49). Indeed, this
431 protective effect could contribute to our observation that SARS-CoV-2 delivered in PBS

(which contains no proteins) resulted in the best virus inactivation whichever copper or Cu_2O-containing surface was tested. We speculate that the absence of proteins in the virus carrier solution could have two consequences (i) as discussed above, more copper ions are available for virus inactivation and (ii) the virus is less stable and thus more vulnerable to the antiviral activities of copper ions. It should be noted however, that over the timeframe of our experiments (30 mins) we did not observe any significant difference in SARS-CoV-2 viability in the different carrier solutions in the absence of copper.

Further investigation is required to understand the results we obtained when virus was delivered in AS (which contains the glycoprotein mucin at 0.3% w/v) (Fig.5), but our observations could suggest that different species of copper ions released from different copper surfaces could affect the degree of copper ion complexation and may also be dependent upon the type and level of chelating biomolecules present. For example, the presence of both ~ 2 mM urea and the thiocynate ions in the AS will be forming various mixed hexadenate complexes with the copper ions in the aqueous solution. Although we did not observe any significant difference in SARS-CoV-2 viability in the presence of the AS formulation used in this study, it should be noted that mucins (0.5-5% w/v) have been reported to inhibit coronavirus infection in a concentration and glycan-dependent (50). Therefore, the effect of mucins in physiologically relevant carrier solutions should be considered when conducting laboratory studies to test surface antiviral performance, particularly as mucin glycan composition and concentration will vary dependent upon the type of respiratory secretion and donor.

454 It is pertinent to stress that composition of virus carrier solution is just one
455 important parameter, alongside multiple other variables, including virus inoculum size,
456 that should be considered when assessing surface antiviral performance (2, 4, 49).
457 Overall, these results further reiterate our conclusion that laboratory testing of surface
458 antiviral performance should include virus delivered in a physiologically relevant carrier
459 solution to replicate a real-life scenario and accurately assess the antiviral performance
460 of test surfaces.
461
462 **Materials and Methods**
463
464 **Generation of metal and metal oxide test surface coupons.** All test surface coupons
465 used are summarized in Tables S1 and S2. Thin film growth by electron beam
466 evaporation was used to generated copper, bismuth and silver films. The films have
467 been grown with various thicknesses using an e-beam evaporator in a vacuum of 10^{-6}
468 mbar. Films were deposited with growth rates of approximately 10 nm/min with the
469 substrate held at room temperature. Growth rates were calibrated using a quartz crystal
470 microbalance. We employed silicon substrates (Inseto) with 5 nm thick nickel-chromium
471 alloy (Ni-Cr) coating as an adhesion layer before growing the metals on top. The
472 samples were cut into 4x4 mm^2 pieces after growth to provide coupons for SARS-CoV-2
473 inactivation assays.
474 Thin film growth by molecular beam epitaxy was used to deposit palladium,
475 nickel and transition metal oxide films. The films were grown using a reactive oxide
476 molecular beam epitaxy system (MBE) (DCA Instruments Oy., Finland, dual R450),

using thermal effusion cells, as well as an e-beam evaporator to evaporate the elemental metals. Metal films were grown in ultra-high vacuum at a pressure of ~ 1 x 10^{-9} mbar, and oxide compounds in either molecular oxygen or 10 % ozone gas environment. Growth rates were calibrated using a quartz crystal microbalance prior to growth. Film thicknesses are controlled through the growth time. The typical pressure during growth varied from 2 x 10^{-7} to 2 x 10^{-5} mbar, depending on the materials. Samples were stored in a vacuum desiccator before use to avoid degradation due to exposure to air. Glass substrates (Nano Quartz Wafer GmbH, Germany) with a size of 4x4 mm^2 were used for fabricating most of the surfaces, while aluminium oxide (Al_2O_3) (0001) substrates (MaTeck GmbH, Germany, of the same size) were used for copper chromate ($CuCrO_2$). We have also used single crystalline substrates $(LaAlO_3)0.3(Sr_2TaAlO_6)$ (LSAT) (001), 4x4 mm^2, from CrysTec GmbH, Germany) for identifying the crystalline phases using X-ray diffraction (XRD).

Thin film growth by magnetron sputtering was used to generate indium tin oxide (ITO) films, which were obtained from RF sputtering (Nexdep 030 DC/RF magnetron sputtering system, Angstrom Engineering Ltd., Canada) at 200 °C on glass substrates with a size of 4x4mm^2. The total pressure of the argon environment was kept at ~ 3 mTorr during the growth, and the films were annealed for 30 min after the sputtering.

For reference purposes we have included bulk foils of copper and stainless steel in the deactivation experiments. Copper foils of various thicknesses (Cu purity 99.9 %) and stainless steel (AISI 304) plates were obtained from GoodFellow Ltd., UK.

Structural and morphological characterization of thin films. Film thicknesses were confirmed using a profilometer. X-ray diffraction (CuKα, 50 kV, Bruker Corp., USA, Discover D8) was used for phase identification of the materials and for obtaining crystallographic information such as grain size and orientation of the films (Fig. S1). To examine the elemental distribution along the thickness direction (Fig. S2), cross-sectional energy dispersive X-ray spectroscopy (EDX) (Thermo Fisher Scientific Inc., USA (formerly FEI) Titan Themis), performed in a transmission electron microscope (TEM), was utilised. The microscope was operated at 200 kV.

Propagation of SARS-CoV-2 stocks. SARS-CoV-2 strain hCOV-19/England/2/2020 (kind gift of Dr Marian Killip, Public Health England, UK) was used within a class II Microbiology safety cabinet (MSC) inside a Biosafety Level 3 (BSL3) biocontainment facility. SARS-CoV-2 high titre stocks were propagated in Vero E6 cells (African green monkey kidney epithelial cell, ECACC, 85020206) as previously described (51). Briefly, Vero E6 cells were infected at a multiplicity of infection (MOI) of 0.01 and cells cultured in Dulbecco's Modified Eagle's Medium supplemented in 2% v/v FBS (DMEM-2%FBS) for 72 hours post-infection. Virus containing supernatant was collected and clarified by centrifugation for 15 mins at 3,200 x g at 4°C. The clarified stock was either directly aliquoted, flash frozen in liquid nitrogen and stored at -80°C or further concentrated using a polyethylene glycol (PEG) virus precipitation kit (Abcam) according to the manufacturer's instructions. Briefly, 5 x PEG solution was mixed with clarified supernatant (1:4 ratio), incubated at 4°C overnight and then centrifuged at 3,200 x g for 30 minutes at 4°C. The resultant virus containing pellet was resuspended in DMEM-

522 2%FBS using 1/100 volume of the starting virus supernatant and the resultant PEG-
523 stock was then aliquoted, flash frozen in liquid nitrogen and stored at -80°C.
524
525 **Quantitation of viable SARS-CoV-2.** Plaque assay was used, as previously described
526 (51), to determine the titre of SARS-CoV-2 stocks as PFU/mL and to determine the %
527 survival of SARS-CoV-2 following exposure to test antiviral surfaces. All plaques assays
528 were performed in triplicate, plaques manually counted, followed by mean and SD
529 determination. Plaque assay limit of detection (LOD) was determined via a 9-point 1:2
530 serial dilution of SARS-CoV-2 PEG-stock (that prior to the dilution series was diluted
531 1:1000 in DMEM-2%FBS to 5.8 x 10^5 PFU/mL) to achieve theoretical zero. The SARS-
532 CoV-2 plaque assay was performed, and plaque count plotted against dilution to
533 generate a calibration curve. LOD was calculated with the following equation: LOD = 3 x
534 (σ/S), with σ SD and S = slope of calibration curve R^2= 0.9 (52).
535
536 **Test surface SARS-CoV-2 inactivation assay.** Test surfaces (4x4 mm^2 coupons) were
537 disinfected in 70% v/v ethanol and allowed to air dry in a class II MSC for 15 minutes
538 before transfer into 96-well plates using inverted forceps. A 7 μL droplet of SARS-CoV-2
539 virus inoculum containing ~4000 PFU (derived from PEG-stock (5.8 x 10^8 PFU/mL)
540 diluted 1:1000 in DMEM-2%FBS) was pipetted onto the centre of each test coupon and
541 incubated for the indicated times at room temperature. No coupon controls were
542 conducted in parallel, were the equivalent 7 μL of virus inoculum was pipetted into
543 sterile 1.5 mL tubes and incubated for the same length of time as corresponding
544 inoculated test coupons. Recovery of virus from test surfaces was performed by adding

250 µL DMEM-2%FBS and gently pipetting up and down 25 times. The no coupon control was similarly processed. Recovered virus was transferred into individual wells of a 96 well plate and a 10-fold serial dilution in DMEM-2%FBS prepared to facilitate quantitation of % SARS-CoV-2 survival via plaque assay. To test the effect of various virus carrier solutions the SARS-CoV-2 PEG-stock (titre = 5.8 x 10^8 PFU/mL) was utilized. In parallel, the PEG-stock stock was diluted 1:1000 in 3 different carrier virus solution (i) DMEM-2%FBS (ii) PBS or (iii) artificial saliva solution (AS; 0.18 mM $MgCl_2.7H_2O$, 1 mM $CaCl_2.H_2O$, 5 mM $NaHCO_3$, 1.5 mM KH_2PO_4, 2.4 mM K_2HPO_4, 2 mM NH_4Cl, 1.9 mM KSCN, 2 mM $(NH_2)_2CO$, 15 mM NaCl, 14 mM KCl, 0.3% w/v bovine salivary gland mucin (42). A droplet of 7 µL of virus in each carrier solution was verified by plaque assay to contain ~4000 PFU and therefore the test surface virus inactivation assay was conducted as described above. The SARS-CoV-2 survival value was calculated as a percentage of the no coupon control sample and plotted as a bar chart as mean with SD and statistical significance assessed using two-way ANOVA with Tukey's multiple comparison using Prism 9.5 GraphPad software. Significance is reported by P value *, $p < 0.1$, **, $p < 0.01$***, $p < 0.001$, ****, $p < 0.0001$. Alternatively, the data is presented as log reduction in Fig.S4-8.

De-coupled ion dissolution SARS-CoV-2 inactivation assay. To investigate the role of ion dissolution from test surfaces in SARS-CoV-2 inactivation, we performed a variation of the test surface inactivation assay described above, in which virus inactivation is decoupled from the test surface. Test surfaces were disinfected and dried as described above and 7 µL of each carrier solution (DMEM-2%FBS, PBS and AS)

without virus, were pipetted onto the centre of each test coupon and incubated for 0 and 30 minutes at room temperature. No coupon controls were conducted in parallel, were the equivalent 7 μL of each carrier solution was pipetted into sterile 1.5 mL tubes and incubated for the same length of time as corresponding test coupons. After the indicated incubation times, the carrier solution was recovered from the test surface, transferred to 1.5mL tube and spiked with 2 μL of clarified SARS-CoV-2 stock (6 x 10^6 PFU/mL) stock which had been diluted 1:3 in DMEM-2%FBS such that 2 μL contains ~4000 PFU. SARS-CoV-2 incubation in each carrier solution pre-exposed to the test surfaces was performed for a further 0 or 30 minutes, followed by transfer into 96-well plates to facilitate quantitation of % SARS-CoV-2 survival by plaque assay as described above.

Inductively Coupled Plasma - Optical Emission Spectroscopy (ICP-OES). ICP-OES was used to determine Cu ion concentration dissolved into carrier solution (DMEM-2%FBS, PBS or AS) upon exposure to various copper test surfaces. Prior to analysis test surfaces were disinfected and dried as described above and 7μL of each carrier solution added for 30 min at room temperature and then recovered in a further 250 μL of carrier solution, which was diluted 10X with 5% nitric acid. Alongside test samples, carrier solution controls not exposed to test surfaces, cupric acetate (~90 ppm Cu ions) positive control and calibration standards (0, 0.005, 0.02 and 0.1 ppm Cu ions) were analysed. All analysis was conducted by The University of Edinburgh ICP analysis facility using a Vista-PRO Simultaneous ICP-OES (Varian/Agilent). LOD was calculated with the following equation: LOD = 3 x (σ/S), with σ = SD and S = slope of calibration curve R^2= 0.9.

Acknowledgments

This work was funded by UKRI-NIHR (MRC MR/V028464/1) COVID-19 Rapid Response Initiative. This grant was awarded to PW, CSA, TKS, PDCK, ADF. The funders have no role in the study, design, data collection and interpretation, or the decision to submit the work for publication. For the purpose of open access, the author(s) has applied a Creative Commons Attribution (CC BY) licence to any Accepted Manuscript version arising.

Author contributions: PW, CSA TKS, PDCK and ADF conceived the study. JH, YN, MF, MA, ADF, CSA executed the experiments. All authors analysed and interpreted the experimental data. CSA, PW, TKS, PDCK, JH, YN wrote the manuscript.

Underpinning data will made available at reference 48.

References

1. Birkett M, Dover L, Cherian Lukose C, Wasy Zia A, Tambuwala MM, Serrano-Aroca A. 2022. Recent Advances in Metal-Based Antimicrobial Coatings for High-Touch Surfaces. Int J Mol Sci 23.
2. Boone SA, Gerba CP. 2007. Significance of fomites in the spread of respiratory and enteric viral disease. Appl Environ Microbiol 73:1687-96.
3. Leung NHL. 2021. Transmissibility and transmission of respiratory viruses. Nat Rev Microbiol 19:528-545.

4. Geng Y, Wang Y. 2023. Stability and transmissibility of SARS-CoV-2 in the environment. J Med Virol 95:e28103.
5. Goldman E. 2021. SARS Wars: the Fomites Strike Back. Appl Environ Microbiol 87:e0065321.
6. van Doremalen N, Bushmaker T, Morris DH, Holbrook MG, Gamble A, Williamson BN, Tamin A, Harcourt JL, Thornburg NJ, Gerber SI, Lloyd-Smith JO, de Wit E, Munster VJ. 2020. Aerosol and Surface Stability of SARS-CoV-2 as Compared with SARS-CoV-1. N Engl J Med 382:1564-1567.
7. Pastorino B, Touret F, Gilles M, de Lamballerie X, Charrel RN. 2020. Prolonged Infectivity of SARS-CoV-2 in Fomites. Emerg Infect Dis 26.
8. Zhou J, Otter JA, Price JR, Cimpeanu C, Meno Garcia D, Kinross J, Boshier PR, Mason S, Bolt F, Holmes AH, Barclay WS. 2021. Investigating Severe Acute Respiratory Syndrome Coronavirus 2 (SARS-CoV-2) Surface and Air Contamination in an Acute Healthcare Setting During the Peak of the Coronavirus Disease 2019 (COVID-19) Pandemic in London. Clin Infect Dis 73:e1870-e1877.
9. Colaneri M, Seminari E, Novati S, Asperges E, Biscarini S, Piralla A, Percivalle E, Cassaniti I, Baldanti F, Bruno R, Mondelli MU, Force CISMPT. 2020. Severe acute respiratory syndrome coronavirus 2 RNA contamination of inanimate surfaces and virus viability in a health care emergency unit. Clin Microbiol Infect 26:1094 e1-1094 e5.

10. Onakpoya IJ, Heneghan CJ, Spencer EA, Brassey J, Pluddemann A, Evans DH, Conly JM, Jefferson T. 2021. SARS-CoV-2 and the role of fomite transmission: a systematic review. F1000Res 10:233.
11. Santarpia JL, Rivera DN, Herrera VL, Morwitzer MJ, Creager HM, Santarpia GW, Crown KK, Brett-Major DM, Schnaubelt ER, Broadhurst MJ, Lawler JV, Reid SP, Lowe JJ. 2020. Aerosol and surface contamination of SARS-CoV-2 observed in quarantine and isolation care. Sci Rep 10:12732.
12. Ahn JY, An S, Sohn Y, Cho Y, Hyun JH, Baek YJ, Kim MH, Jeong SJ, Kim JH, Ku NS, Yeom JS, Smith DM, Lee H, Yong D, Lee YJ, Kim JW, Kim HR, Hwang J, Choi JY. 2020. Environmental contamination in the isolation rooms of COVID-19 patients with severe pneumonia requiring mechanical ventilation or high-flow oxygen therapy. J Hosp Infect 106:570-576.
13. Grass G, Rensing C, Solioz M. 2011. Metallic copper as an antimicrobial surface. Appl Environ Microbiol 77:1541-7.
14. Ramos-Zuniga J, Bruna N, Perez-Donoso JM. 2023. Toxicity Mechanisms of Copper Nanoparticles and Copper Surfaces on Bacterial Cells and Viruses. Int J Mol Sci 24.
15. Salah I, Parkin IP, Allan E. 2021. Copper as an antimicrobial agent: recent advances. RSC Adv 11:18179-18186.
16. Liu LT, Chin AWH, Yu P, Poon LLM, Huang MX. 2022. Anti-pathogen stainless steel combating COVID-19. Chem Eng J 433:133783.

17. Mosselhy DA, Kareinen L, Kivisto I, Aaltonen K, Virtanen J, Ge Y, Sironen T. 2021. Copper-Silver Nanohybrids: SARS-CoV-2 Inhibitory Surfaces. Nanomaterials (Basel) 11.
18. Meister TL, Fortmann J, Breisch M, Sengstock C, Steinmann E, Koller M, Pfaender S, Ludwig A. 2022. Nanoscale copper and silver thin film systems display differences in antiviral and antibacterial properties. Sci Rep 12:7193.
19. Mantlo EK, Paessler S, Seregin A, Mitchell A. 2021. Luminore CopperTouch Surface Coating Effectively Inactivates SARS-CoV-2, Ebola Virus, and Marburg Virus In Vitro. Antimicrob Agents Chemother 65:e0139020.
20. Hutasoit N, Kennedy B, Hamilton S, Luttick A, Rahman Rashid RA, Palanisamy S. 2020. Sars-CoV-2 (COVID-19) inactivation capability of copper-coated touch surface fabricated by cold-spray technology. Manuf Lett 25:93-97.
21. Terzioglu E, Arslan M, Balaban BG, Cakar ZP. 2022. Microbial silver resistance mechanisms: recent developments. World J Microbiol Biotechnol 38:158.
22. Manakhov AM, Permyakova ES, Sitnikova NA, Tsygankova AR, Alekseev AY, Solomatina MV, Baidyshev VS, Popov ZI, Blahova L, Elias M, Zajickova L, Kovalskii AM, Sheveyko AN, Kiryukhantsev-Korneev PV, Shtansky DV, Necas D, Solovieva AO. 2022. Biodegradable Nanohybrid Materials as Candidates for Self-Sanitizing Filters Aimed at Protection from SARS-CoV-2 in Public Areas. Molecules 27.
23. Delumeau LV, Asgarimoghaddam H, Alkie T, Jones AJB, Lum S, Mistry K, Aucoin MG, DeWitte-Orr S, Musselman KP. 2021. Effectiveness of antiviral metal

677 and metal oxide thin-film coatings against human coronavirus 229E. APL Mater
678 9:111114.
679 24. Jeremiah SS, Miyakawa K, Morita T, Yamaoka Y, Ryo A. 2020. Potent antiviral
680 effect of silver nanoparticles on SARS-CoV-2. Biochem Biophys Res Commun
681 533:195-200.
682 25. Galdiero S, Falanga A, Vitiello M, Cantisani M, Marra V, Galdiero M. 2011. Silver
683 nanoparticles as potential antiviral agents. Molecules 16:8894-918.
684 26. Kumar A, Nath K, Parekh Y, Enayathullah MG, Bokara KK, Sinhamahapatra A.
685 2021. Antimicrobial silver nanoparticle-photodeposited fabrics for SARS-CoV-2
686 destruction. Colloid Interface Sci Commun 45:100542.
687 27. He Q, Lu J, Liu N, Lu W, Li Y, Shang C, Li X, Hu L, Jiang G. 2022. Antiviral
688 Properties of Silver Nanoparticles against SARS-CoV-2: Effects of Surface
689 Coating and Particle Size. Nanomaterials (Basel) 12.
690 28. Baselga M, Uranga-Murillo I, de Miguel D, Arias M, Sebastian V, Pardo J,
691 Arruebo M. 2022. Silver Nanoparticles-Polyethyleneimine-Based Coatings with
692 Antiviral Activity against SARS-CoV-2: A New Method to Functionalize Filtration
693 Media. Materials (Basel) 15.
694 29. Bono N, Ponti F, Punta C, Candiani G. 2021. Effect of UV Irradiation and TiO2-
695 Photocatalysis on Airborne Bacteria and Viruses: An Overview. Materials (Basel)
696 14.
697 30. Micochova P, Chadha A, Hesseloj T, Fraternali F, Ramsden JJ, Gupta RK. 2021.
698 Rapid inactivation of SARS-CoV-2 by titanium dioxide surface coating. Wellcome
699 Open Res 6:56.

31. Nakano R, Yamaguchi A, Sunada K, Nagai T, Nakano A, Suzuki Y, Yano H, Ishiguro H, Miyauchi M. 2022. Inactivation of various variant types of SARS-CoV-2 by indoor-light-sensitive TiO2-based photocatalyst. Sci Rep 12:5804.
32. Matsuura R, Lo CW, Wada S, Somei J, Ochiai H, Murakami T, Saito N, Ogawa T, Shinjo A, Benno Y, Nakagawa M, Takei M, Aida Y. 2021. SARS-CoV-2 Disinfection of Air and Surface Contamination by TiO2 Photocatalyst-Mediated Damage to Viral Morphology, RNA, and Protein. Viruses 13.
33. Han R, Coey JD, O'Rourke C, Bamford CGG, Mills A. 2022. Flexible, disposable photocatalytic plastic films for the destruction of viruses. J Photochem Photobiol B 235:112551.
34. Lu Y, Guan S, Hao L, Yoshida H, Nakada S, Takizawa T, Itoi T. 2022. Inactivation of SARS-CoV-2 and photocatalytic degradation by TiO2 photocatalyst coatings. Sci Rep 12:16038.
35. Hosseini M, Chin AWH, Williams MD, Behzadinasab S, Falkinham JO, 3rd, Poon LLM, Ducker WA. 2022. Transparent Anti-SARS-CoV-2 and Antibacterial Silver Oxide Coatings. ACS Appl Mater Interfaces 14:8718-8727.
36. Gentili V, Pazzi D, Rizzo S, Schiuma G, Marchini E, Papadia S, Sartorel A, Di Luca D, Caccuri F, Bignozzi CA, Rizzo R. 2021. Transparent Polymeric Formulations Effective against SARS-CoV-2 Infection. ACS Appl Mater Interfaces 13:54648-54655.
37. Behzadinasab S, Williams MD, Hosseini M, Poon LLM, Chin AWH, Falkinham JO, 3rd, Ducker WA. 2021. Transparent and Sprayable Surface Coatings that Kill

722 Drug-Resistant Bacteria Within Minutes and Inactivate SARS-CoV-2 Virus. ACS
723 Appl Mater Interfaces 13:54706-54714.
724 38. Hosseini M, Chin AWH, Behzadinasab S, Poon LLM, Ducker WA. 2021. Cupric
725 Oxide Coating That Rapidly Reduces Infection by SARS-CoV-2 via Solids. ACS
726 Appl Mater Interfaces 13:5919-5928.
727 39. Behzadinasab S, Chin A, Hosseini M, Poon L, Ducker WA. 2020. A Surface
728 Coating that Rapidly Inactivates SARS-CoV-2. ACS Appl Mater Interfaces
729 12:34723-34727.
730 40. Merkl P, Long S, McInerney GM, Sotiriou GA. 2021. Antiviral Activity of Silver,
731 Copper Oxide and Zinc Oxide Nanoparticle Coatings against SARS-CoV-2.
732 Nanomaterials (Basel) 11.
733 41. Purniawan A, Lusida MI, Pujiyanto RW, Nastri AM, Permanasari AA, Harsono
734 AAH, Oktavia NH, Wicaksono ST, Dewantari JR, Prasetya RR, Rahardjo K,
735 Nishimura M, Mori Y, Shimizu K. 2022. Synthesis and assessment of copper-
736 based nanoparticles as a surface coating agent for antiviral properties against
737 SARS-CoV-2. Sci Rep 12:4835.
738 42. Woo MH, Hsu YM, Wu CY, Heimbuch B, Wander J. 2010. Method for
739 contamination of filtering facepiece respirators by deposition of MS2 viral
740 aerosols. J Aerosol Sci 41:944-952.
741 43. Diaz-Arnold AM, Marek CA. 2002. The impact of saliva on patient care: A
742 literature review. J Prosthet Dent 88:337-43.

44. Hedberg J, Karlsson HL, Hedberg Y, Blomberg E, Odnevall Wallinder I. 2016. The importance of extracellular speciation and corrosion of copper nanoparticles on lung cell membrane integrity. Colloids Surf B Biointerfaces 141:291-300.
45. Sharan R, Chhibber S, Attri S, Reed RH. 2010. Inactivation and sub-lethal injury of Escherichia coli in a copper water storage vessel: effect of inorganic and organic constituents. Antonie Van Leeuwenhoek 98:103-15.
46. Glover CF, Miyake T, Wallemacq V, Harris JD, Emery J, Engel DA, McDonnell SJ, Scully JR. 2022. Interrogating the Effect of Assay Media on the Rate of Virus Inactivation of High-Touch Copper Surfaces: A Materials Science Approach. Advanced Materials Interfaces 9.
47. Behzadinasab S, Williams MD, Falkinham Iii JO, Ducker WA. 2023. Antimicrobial mechanism of cuprous oxide (Cu(2)O) coatings. J Colloid Interface Sci 652:1867-1877.
48. Hans M, Erbe A, Mathews S, Chen Y, Solioz M, Mucklich F. 2013. Role of copper oxides in contact killing of bacteria. Langmuir 29:16160-6.
49. Bangiyev R, Chudaev M, Schaffner DW, Goldman E. 2021. Higher Concentrations of Bacterial Enveloped Virus Phi6 Can Protect the Virus from Environmental Decay. Appl Environ Microbiol 87:e0137121.
50. Wardzala CL, Wood AM, Belnap DM, Kramer JR. 2022. Mucins Inhibit Coronavirus Infection in a Glycan-Dependent Manner. ACS Cent Sci 8:351-360.
51. Gruschow S, Adamson CS, White MF. 2021. Specificity and sensitivity of an RNA targeting type III CRISPR complex coupled with a NucC endonuclease effector. Nucleic Acids Res 49:13122-13134.

52. Sengul U. 2016. Comparing determination methods of detection and quantification limits for aflatoxin analysis in hazelnut. J Food Drug Anal 24:56-62.

Figure legends

FIG 1 SARS-CoV-2 inactivation upon exposure to copper surfaces over time. (A) Percent survival of SARS-CoV-2 exposed to different metal surfaces after 0-, 30-, 60- and 120-min. Data is expressed as a percentage of a no coupon control at 0-min time point for each test condition. Data shown represents mean values (n = 3 replicates and error bar = SD) and is representative of 3 independent experiments. Statistical significance was assessed using two-way ANOVA with Tukeys multiple comparison test, **** $p < 0.0001$. The limit of detection (LOD) for the assay is indicated by the solid red line and 50% inactivation is indicated by the black dotted line. (B) Titre of SARS-CoV-2 (PFU/mL) exposed to different test surfaces as a function of time, exponential fits to the data are shown along with a solid red line, which indicates the LOD for the assay.

FIG 2 Screening test elemental metal and metal oxide surfaces for SARS-CoV-2 antiviral activity superior to copper. Percent survival of SARS-CoV-2 exposed to different test metal and metal oxide surfaces after 0 and 30 min compared to no coupon, stainless steel, and copper controls. Data is expressed as a percentage of a no coupon control at 0 min time point for each test condition. (A) elemental metal test surfaces; silver (Ag), nickel (Ni), palladium (Pd), bismuth (Bi) (B) metal oxide test

surfaces; copper chromate ($CuCrO_2$), titanium oxide (TiO_2), indium tin oxide (ITO) and (C) copper oxide test surfaces; annealed evaporated copper (CuO/Cu_2O mixture) and predominantly Cu_2O containing surfaces, generated at indicated thicknesses. Data shown represents mean values (n = 3 replicates and error bar = SD) and is representative of 3 independent experiments. Statistical significance was assessed using two-way ANOVA with Tukeys multiple comparison test, **** $p < 0.0001$, ** $p < 0.01$, * $p < 0.1$. The limit of detection (LOD) for the assay is indicated by the solid red line and 50% inactivation is indicated by the black dotted line.

FIG 3 Effect of copper surface film thickness on SARS-CoV-2 inactivation. (A) Percent survival of SARS-CoV-2 exposed to coupons with evaporated copper film of increasing thickness. Data shown represents mean values (n = 3 replicates and error bar = SD) and is representative of 3 independent experiments. The limit of detection (LOD) for the assay is indicated by the solid red line and 50% inactivation is indicated by the black dotted line. (B) images of evaporated copper thin-film coupons of 50 nm and 500 nm thicknesses before, during and after 30 min incubation with a 7 μL droplet of DMEM-2%FBS.

FIG 4 Impact of different carrier solutions on copper ion dissolution and SARS-CoV-2 inactivation upon exposure to an evaporated copper thin-film surface. (A) ICP-OES determined copper ion levels in DMEM-2%FBS, PBS or AS carrier solutions following 30-mi exposure to evaporated copper, Cu_2O thin film coupons or no coupon control. Data shown represents mean values (n = 6 replicates and error bar = SD). (B-D)

812 percent survival of SARS-CoV-2 resuspended in DMEM-2%FBS, PBS or AS carrier
813 solutions and exposed to evaporated copper surfaces for (B) 30, (C) 20 and (D) 10 min
814 or the equivalent no coupon control. Data is expressed as a percentage of a no coupon
815 control at 0 min time point for each test condition. Data shown represents mean values
816 (n = 3 replicates and error bar = SD). At the 30 min time point the data shown is
817 representative of 3 independent experiments, the 20- and 10-min time points were
818 included in the 3rd and final experimental repeat. Statistical significance was assessed
819 using two-way ANOVA with Tukeys multiple comparison test, **** $p < 0.0001$, *** $p <$
820 0.001. The limit of detection (LOD) for the assay is indicated by the solid red line and
821 50% inactivation is indicated by the black dotted line.
822
823 **FIG 5** De-coupled ion dissolution SARS-CoV-2 inactivation assay. (A and B) test
824 surface virus inactivation assay: percent survival of SARS-CoV-2 resuspended in
825 DMEM-2%FBS, PBS or AS carrier solutions and exposed to (A) evaporated copper or
826 (B) Cu_2O thin-film coupons for 0 or 30 minutes or the equivalent no coupon control. (C
827 and D) de-coupled virus inactivation assay: carrier solution DMEM-2%FBS, PBS or AS
828 exposed to evaporated copper (C) and Cu_2O (D) thin-film coupons for 0 or 30 min or the
829 equivalent no coupon control. Following coupon exposure, the resultant solution is
830 removed and spiked with SARS-CoV-2 and incubated for a further 0 or 30 min or the
831 equivalent no coupon control. Data is shown as percent survival of SARS-CoV-2 is
832 expressed as a percentage of a no coupon control at 0-min time point for each test
833 condition. Data represents mean values (n = 3 replicates and error bar = SD) and is
834 representative of 3 independent experiments. Statistical significance was assessed

using two-way ANOVA with Tukeys multiple comparison test, **** $p < 0.0001$. The limit of detection (LOD) for the assay is indicated by the solid red line and 50% inactivation is indicated by the black dotted line.

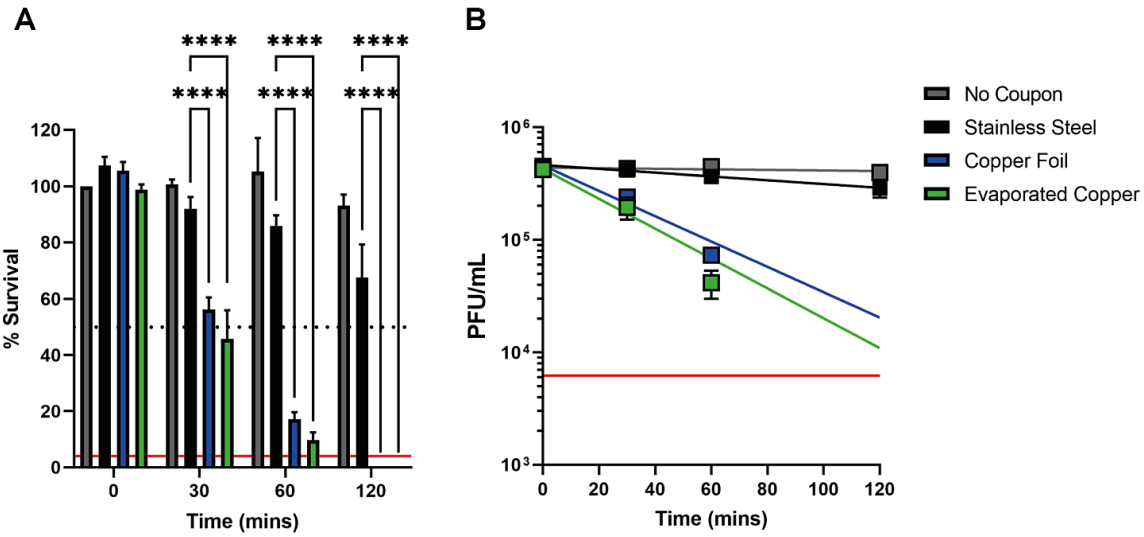
A
B
****
****
****
****
****
****
% Survival
120
100
80
60
40
20
0
0
30
60
120
Time (mins)
PFU/mL
10^6
10^5
10^4
10^3
0
20
40
60
80
100
120
Time (mins)
No Coupon
Stainless Steel
Copper Foil
Evaporated Copper

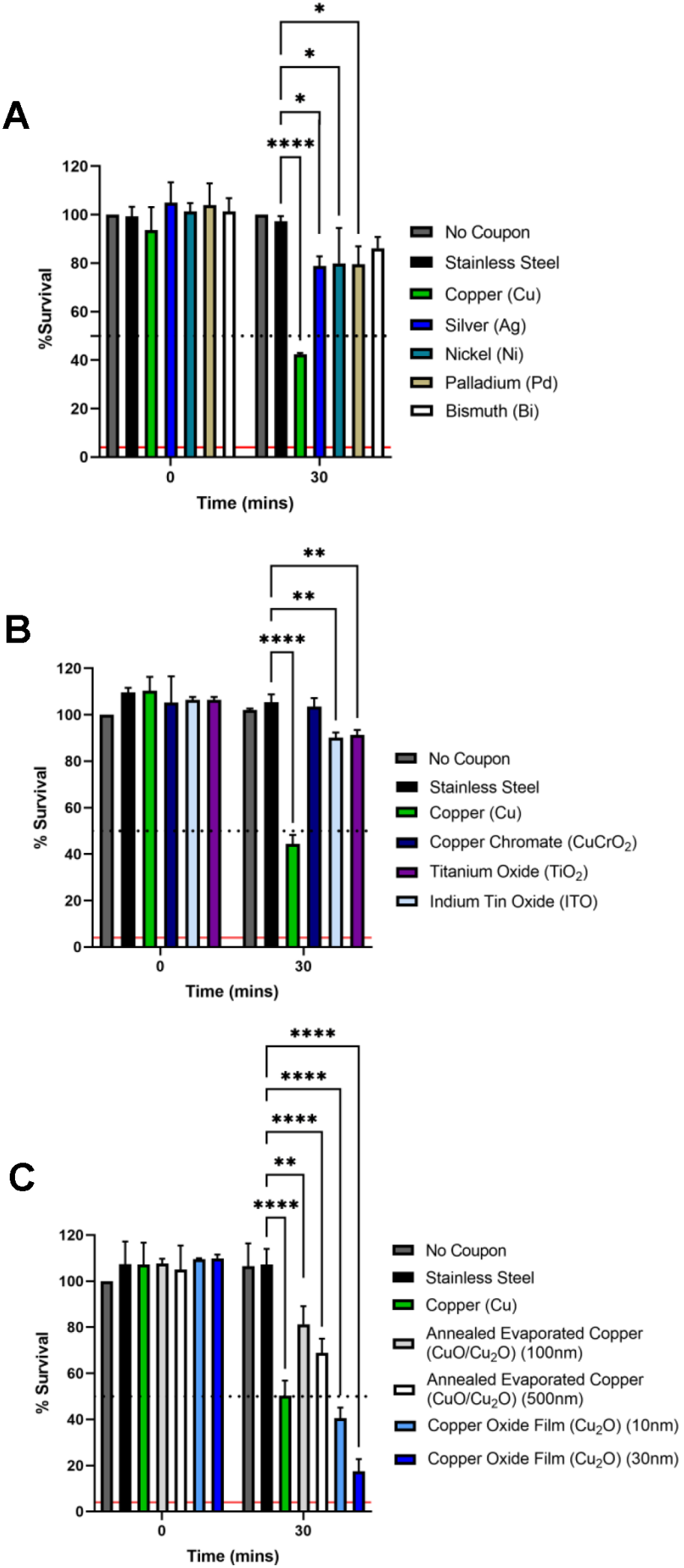
A
*
*
*
****
120
100
80
60
40
20
0
%Survival
0
30
Time (mins)
No Coupon
Stainless Steel
Copper (Cu)
Silver (Ag)
Nickel (Ni)
Palladium (Pd)
Bismuth (Bi)
B
**
**
****
120
100
80
60
40
20
0
% Survival
0
30
Time (mins)
No Coupon
Stainless Steel
Copper (Cu)
Copper Chromate ($CuCrO_2$)
Titanium Oxide (TiO_2)
Indium Tin Oxide (ITO)
C
****
****
****
**
****
120
100
80
60
40
20
0
% Survival
0
30
Time (mins)
No Coupon
Stainless Steel
Copper (Cu)
Annealed Evaporated Copper (CuO/Cu_2O) (100nm)
Annealed Evaporated Copper (CuO/Cu_2O) (500nm)
Copper Oxide Film (Cu_2O) (10nm)
Copper Oxide Film (Cu_2O) (30nm)

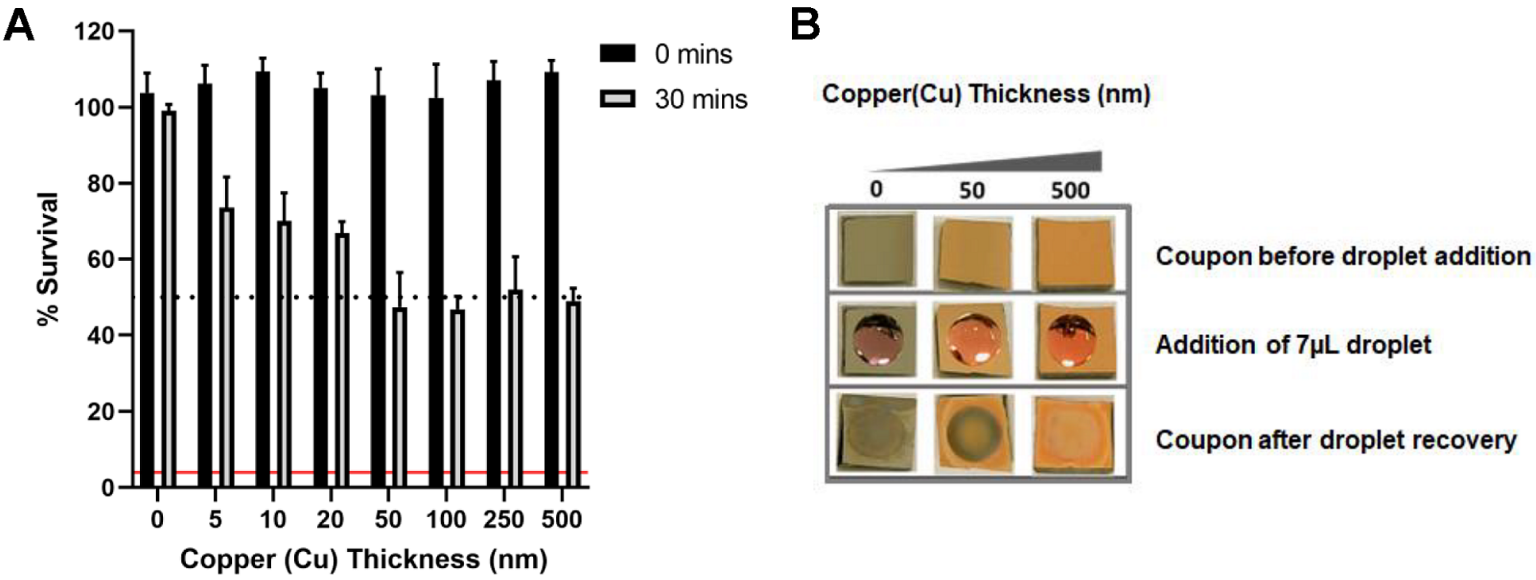
A
120
100
80
60
40
20
0
% Survival
0 mins
30 mins
0
5
10
20
50
100
250
500
Copper (Cu) Thickness (nm)
B
Copper(Cu) Thickness (nm)
0
50
500
Coupon before droplet addition
Addition of 7µL droplet
Coupon after droplet recovery

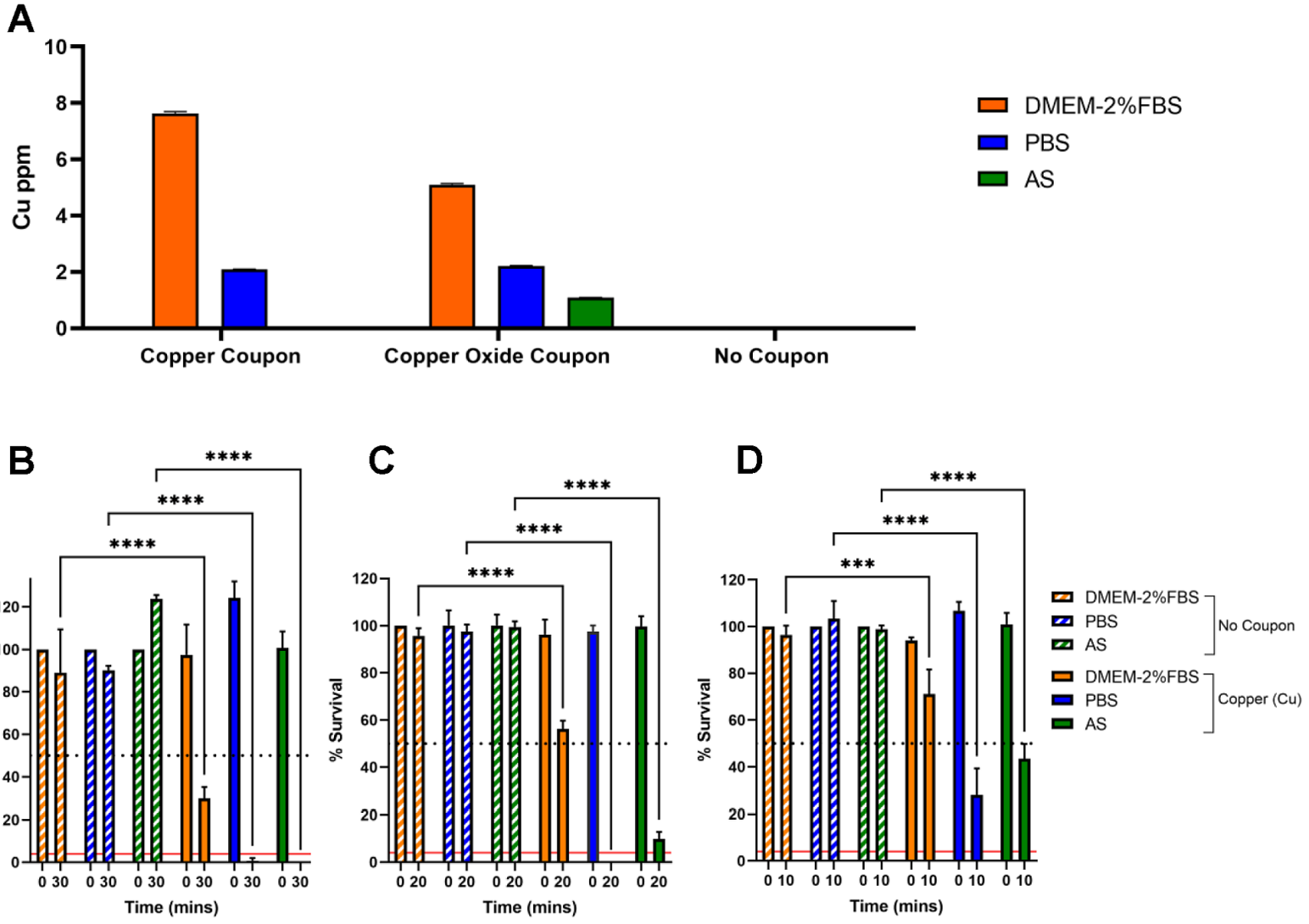
A
Cu ppm
10
8
6
4
2
0
Copper Coupon
Copper Oxide Coupon
No Coupon
DMEM-2%FBS
PBS
AS
B
C
D
% Survival
Time (mins)
****
***
0 30
0 20
0 10
No Coupon
Copper (Cu)

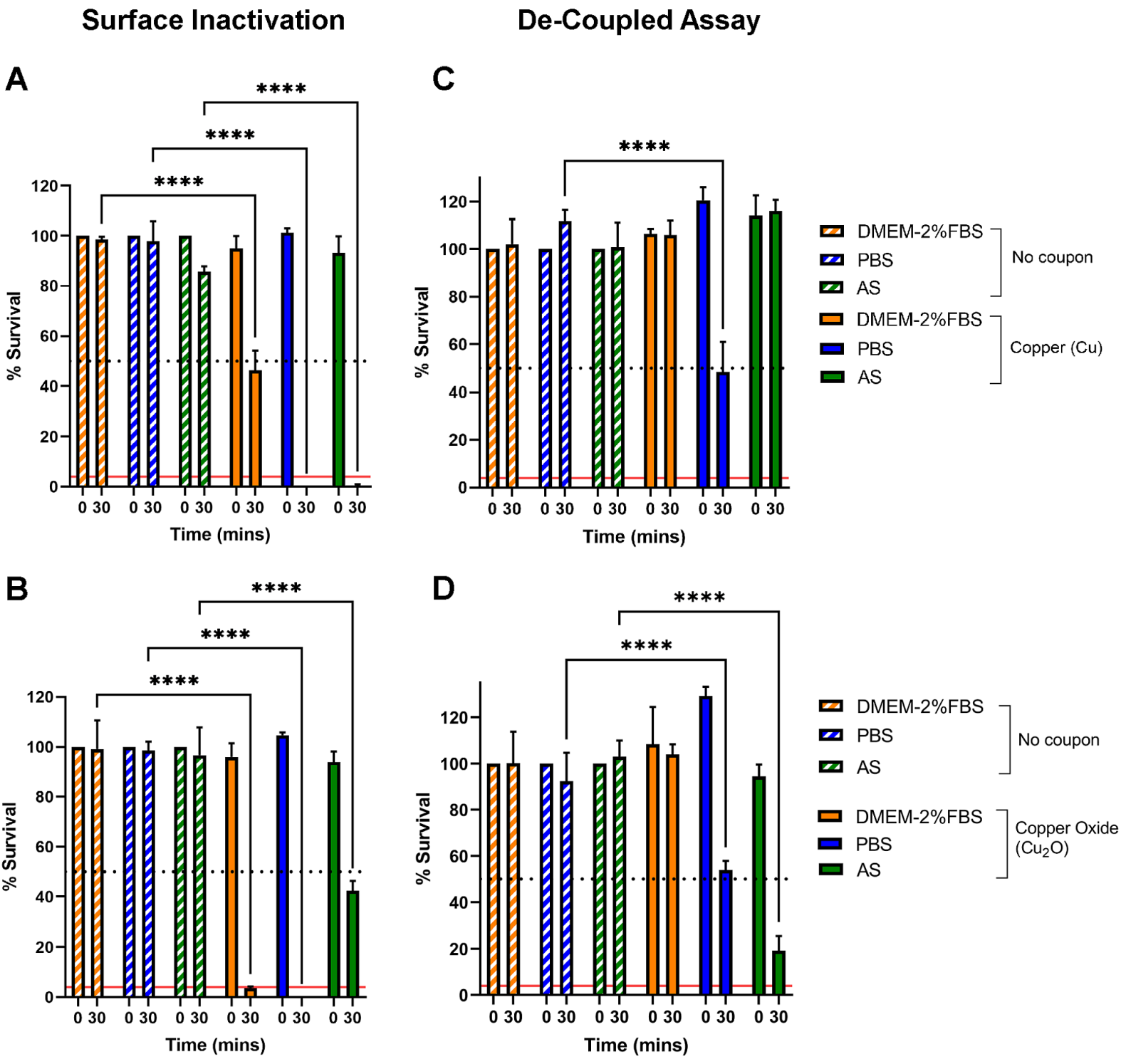
Surface Inactivation
De-Coupled Assay
A
B
C
D
% Survival
Time (mins)
0 30
****
DMEM-2%FBS
PBS
AS
No coupon
Copper (Cu)
Copper Oxide (Cu2O)

Supplementary Material:

The role of ion dissolution in metal and metal oxide surface inactivation of SARS-CoV-2

Jane Hilton[a*], Yoshiko Nanao[b*], Machiel Flokstra[b], Meisam Askari[b$], Terry K. Smith[a] Andrea Di Falco[b] Phil D.C. King[b], Peter Wahl[b#], Catherine S Adamson[a#]

[a] Biomedical Sciences Research Complex, School of Biology, University of St Andrews, St Andrews, Fife, UK

[b] SUPA, School of Physics and Astronomy, University of St Andrews, St Andrews, Fife, UK

Running Head: Surface Inactivation of SARS-CoV-2

[#]Address correspondence to Catherine S Adamson, csa21@st-andrews.ac.uk or Peter Wahl, gpw2@st-andrews.ac.uk

* Jane Hilton and Yoshiko Nanao contributed equally to this work. Author order was determined as Jane Hilton contributed the biological data, presented in the paper, whereas Yoshiko Nanao generated the test surfaces used in the study.

[$] Present Address: Optek Systems, Abingdon, Oxford, UK

Table S1 Summary of surfaces tested in this study as well as substrate materials, growth methods and profiles, and thickness.

Tested Surfaces	Substrate	Growth method	Growth profile	Thickness (nm)
Evaporated Copper (EC)	NiCr/Si	E-beam	Surface was deposited with e-beam in vacuum at room temperature after adhesive layer (Ni-Cr) deposition on Si.	0 – 500
Silver (Ag)	NiCr/Si	E-beam		250
Bismuth (Bi)	NiCr/Si	E-beam		270
Nickel (Ni)	Glass	MBE	Elemental metal sources were thermally evaporated in vacuum at room temperature directly on glass.	30
Palladium (Pd)	Glass	MBE		20
Copper Chromate ($CuCrO_2$)	Al_2O_3	MBE	Cu and Cr was evaporated alternatively. O_2 pressure and substrate temperature was kept at 5 x 10^{-6} mbar and at 800 ^{o}C, respectively.	25
Indium Tin Oxide (ITO)	Glass	RF sputtering	ITO was sputtered at 200 ^{o}C with the total pressure of 3 mTorr, followed by post annealing for 30 min.	10
Titanium Oxide (TiO_2)	Glass	MBE	Ti was evaporated from effusion cell while O_2 pressure and substrate temperature were kept at 5 x 10^{-6} mbar and at 700 ^{o}C, respectively.	16
Annealed Evaporated Copper (CuO/Cu_2O) mixture	NiCr/Si	Annealing in air	Evaporated copper films were rinsed with acetone and 2-propanol for 5 min each, and dried at 200 ^{o}C for 5 min, then placed on hot surface at 350 ^{o}C in air and left for 1 hour. Cooled in air down to 200 ^{o}C then removed from the hot surface. Films were treated with water when required.	100
				500
Copper Oxide (Cu_2O)	Glass LSAT	MBE	Cu was evaporated at 650 ^{o}C in 10 % O_3 environment where total pressure was kept at approx. 2 x 10^{-5} mbar.	10
				30

Table S2 Summary of cutting, processing and storage of the surfaces tested in this study.

Tested Surfaces	Cutting	Pre-processing	Storing after deposition
Evaporated copper (EC)	Manual cut with diamond pen after deposition	Rinsed with acetone then 2-propanol in an ultra sonicator	Air
Silver (Ag)	(as above)	(as above)	(as above)
Bismuth (Bi)	(as above)	(as above)	(as above)
Nickel (Ni)	Precut substrates were used	(as above)	(as above)
Palladium (Pd)	(as above)	(as above)	(as above)
Copper Chromate ($CuCrO_2$)	(as above)	(as above)	N_2 desiccator
Indium Tin Oxide (ITO)	Manual cut with diamond pen after deposition	(as above)	Air
Titanium Oxide (TiO_2)	Precut substrates were used	(as above)	(as above)
Annealed Evaporated Copper (CuO/Cu_2O) mixture	Cut EC coupons were used	Rinsed with water when needed	Vacuum storage
Copper Oxide (Cu_2O)	Precut substrates were used	Rinsed with acetone then 2-propanol in an ultra sonicator	(as above)
Copper foil	Cut with metal cutter	Polished one side, followed by rinsing with acetone, 2-propanol in an ultra sonicator	Air
Stainless steel	(as above)	(as above)	(as above)

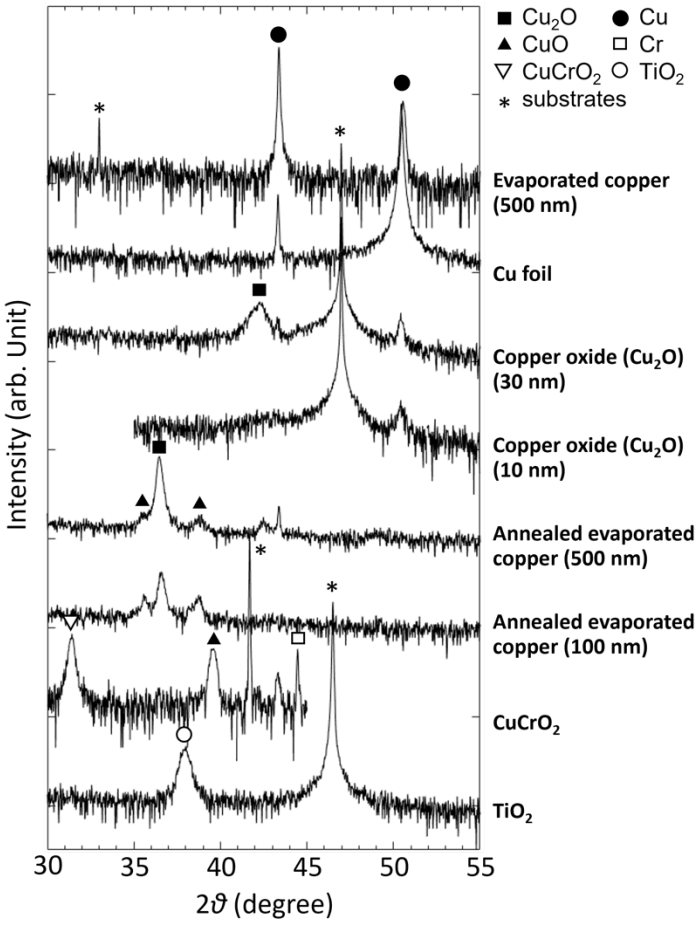

FIG S1 XRD patterns of surfaces tested in this study. Si (1 0 0) with adhesive layer of Ni-Cr alloy was used as a substrate material for films of evaporated copper and annealed copper, while Al_2O_3 (0 0 0 1), $(LaAlO_3)_{0.3}(Sr_2TaAlO_6)_{0.7}$ (LSAT) (0 0 1), and $SrTiO_3$ (0 0 1) were used for stabilising $CuCrO_2$ and binary oxides, respectively. Diffraction peaks from substrate materials are all shown with asterisks (*). Note that the samples of copper oxide and titanium oxide used for virological tests were grown on glass substrates.

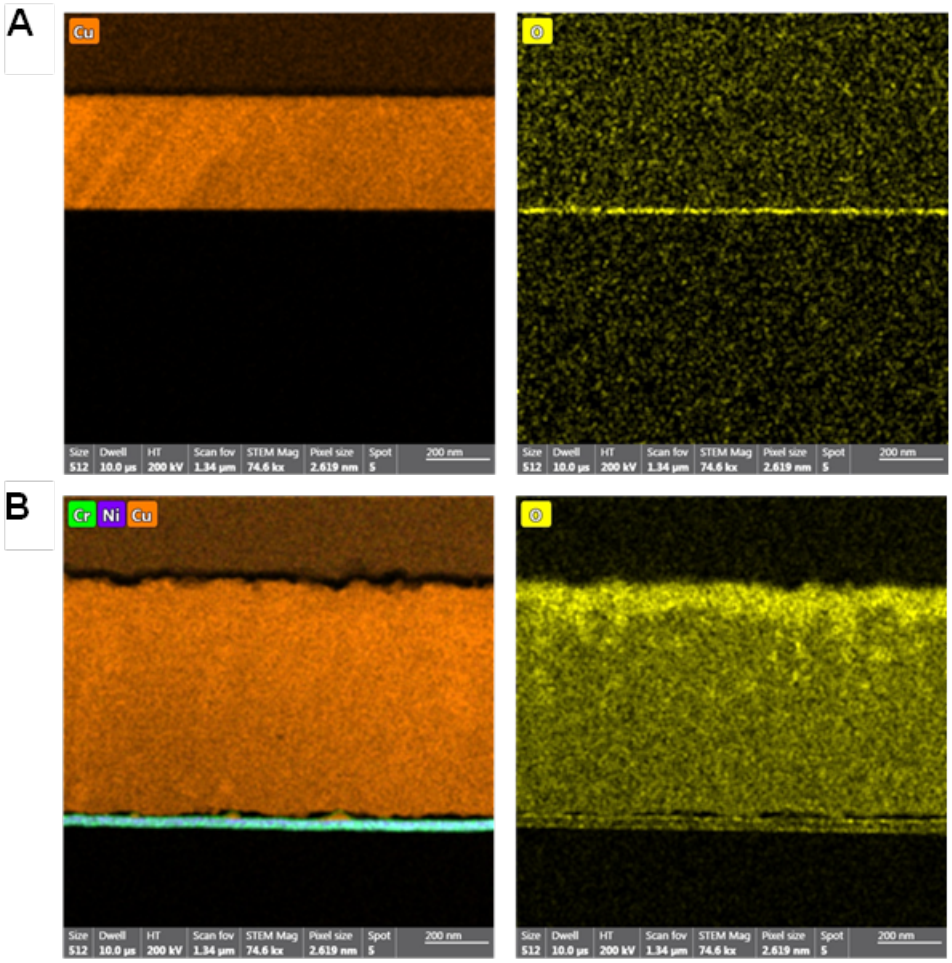

FIG S2 Cross-sectional energy dispersive X-ray analysis images on (A) evaporated copper film on crystalline Si, and (B) annealed evaporated copper. Smooth surface with sharp interface is apparent in images from evaporated copper while the evaporated copper film show rougher surface. Notably, the distribution of oxygen atoms in the annealed copper film (bottom right) is not uniform and higher density of oxygen near the film surface can be seen.

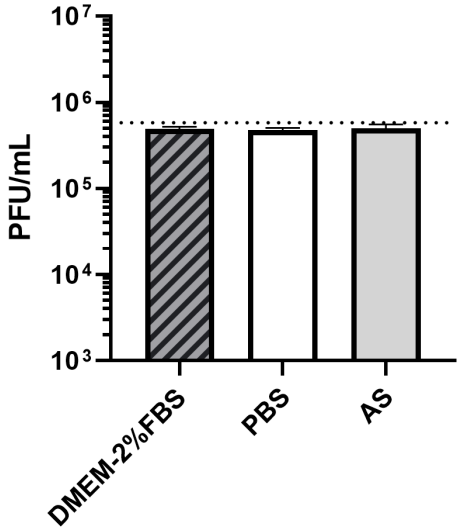

FIG S3 Titre of SARS-CoV-2 in Carrier solutions. Following resuspension of SARS-CoV-2 in each carrier solution, the virus was confirmed as remaining viable. SARS-CoV-2 viral titre was determined, and data is presented as (PFU/mL) in each carrier solution, DMEM-2%FBS, PBS and AS. Data shown represents mean values (n = 3 replicates and error bar = SD) and is representative of 3 independent experiments.

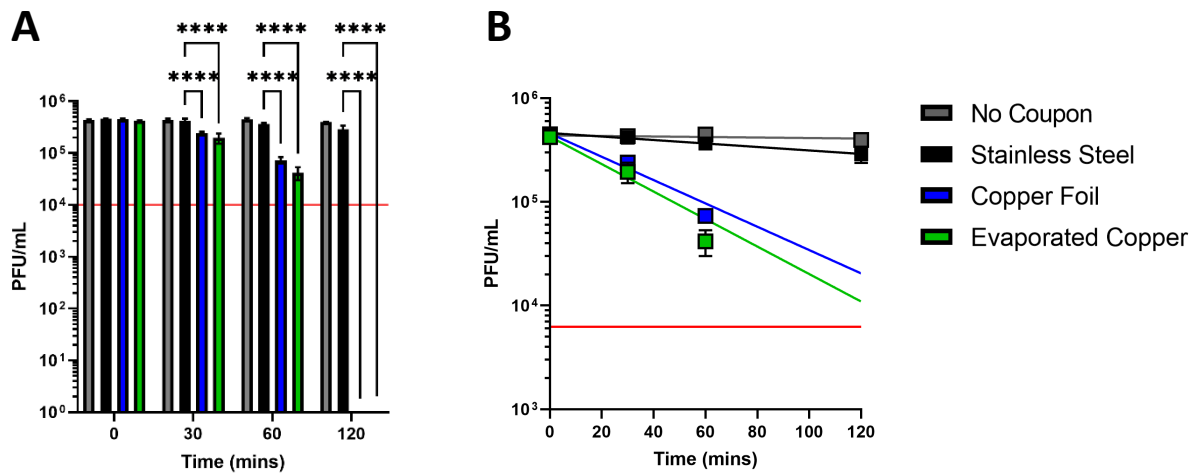

FIG S4 SARS-CoV-2 inactivation upon exposure to copper surfaces over time. (A) Titre of SARS-CoV-2 (PFU/mL) exposed to different metal surfaces after 0-, 30-, 60-and 120-min. Data shown represents mean values (n = 3 replicates and error bar = SD) and is representative of 3 independent experiments. Statistical significance was assessed using two-way ANOVA with Tukeys multiple comparison test, **** $p < 0.0001$. The limit of detection (LOD) for the assay is indicated by the solid red line. (B) Titre of SARS-CoV-2 (PFU/mL) exposed to different test surfaces as a function of time, exponential fits to the data are shown along with a solid red line, which indicates the LOD for the assay.

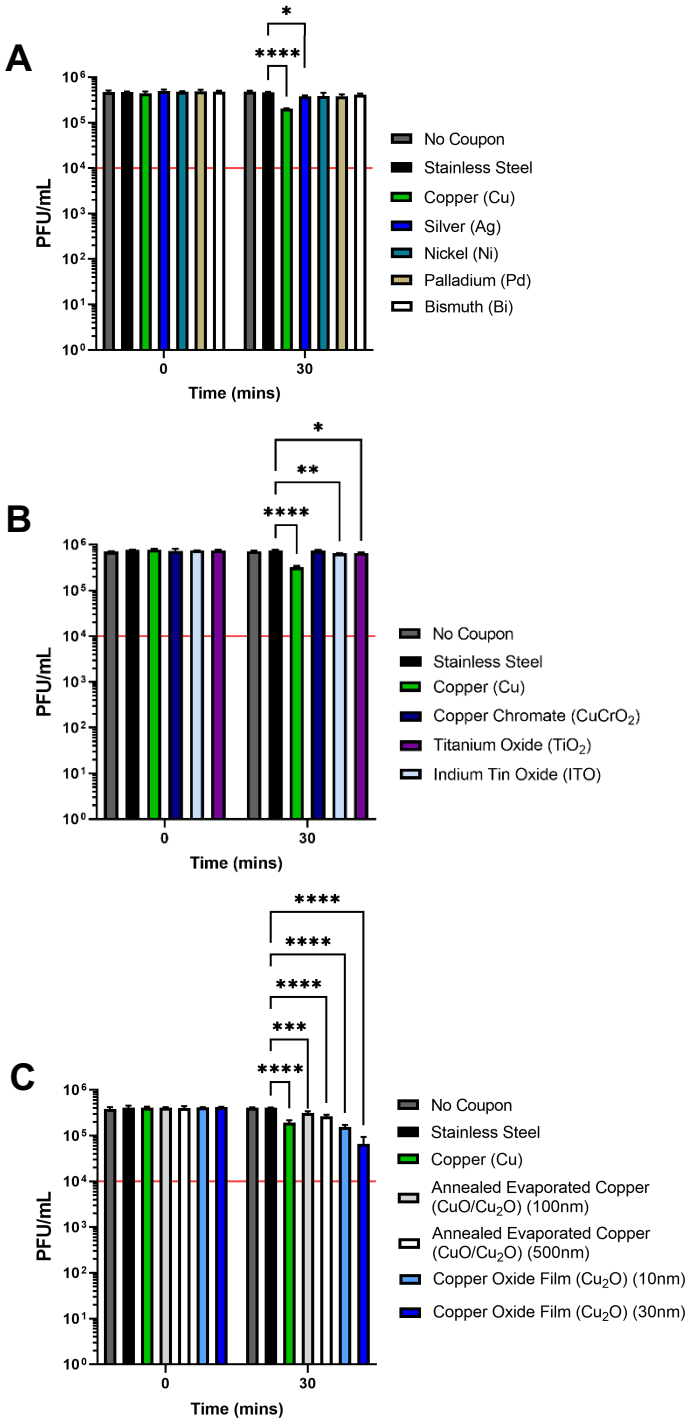

FIG S5 Screening test elemental metal and metal oxide surfaces for SARS-CoV-2 antiviral activity superior to copper. Titre of SARS-CoV-2 (PFU/mL) exposed to different test metal and metal oxide surfaces after 0 and 30 min compared to no coupon, stainless steel, and copper controls. (A) elemental metal test surfaces; silver (Ag), nickel (Ni), palladium (Pd), bismuth (Bi) (B) metal oxide test surfaces; copper chromate ($CuCrO_2$),

titanium oxide (TiO_2), indium tin oxide (ITO) and (C) copper oxide test surfaces; annealed evaporated copper (CuO/Cu_2O mixture) and predominantly Cu_2O containing surfaces, generated at indicated thicknesses. Data shown represents mean values (n = 3 replicates and error bar = SD) and is representative of 3 independent experiments. Statistical significance was assessed using two-way ANOVA with Tukeys multiple comparison test, **** $p < 0.0001$,*** $p < 0.001$, ** $p < 0.01$, * $p < 0.1$. The limit of detection (LOD) for the assay is indicated by the solid red line.

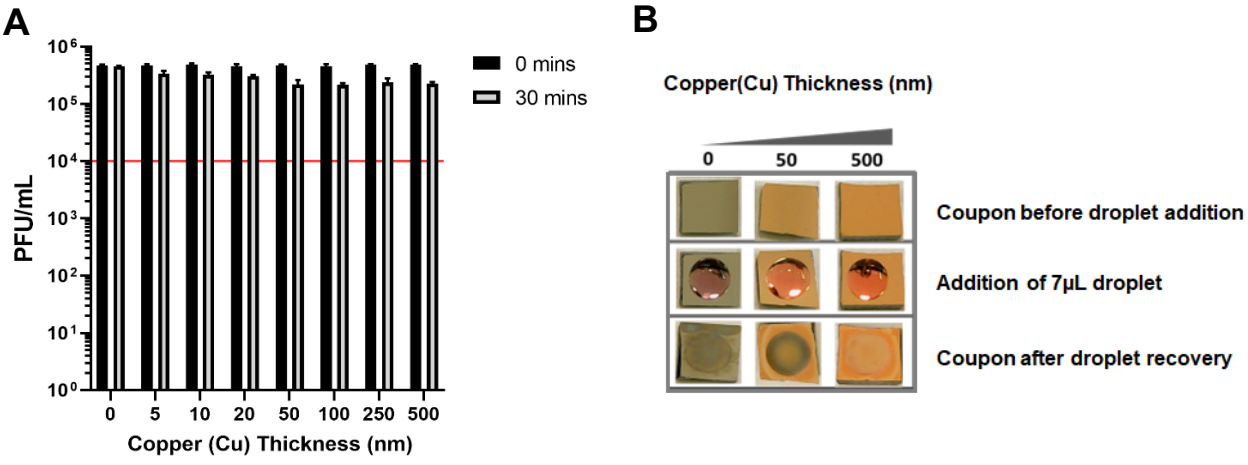

FIG S6 Effect of copper surface film thickness on SARS-CoV-2 inactivation. (A) Titre of SARS-CoV-2 (PFU/mL) exposed to coupons with evaporated copper film of increasing thickness. Data shown represents mean values (n = 3 replicates and error bar = SD) and is representative of 3 independent experiments. The limit of detection (LOD) for the assay is indicated by the solid red line. (B) images of evaporated copper thin-film coupons of 50 nm and 500 nm thicknesses before, during and after 30 min incubation with a 7 µL droplet of DMEM-2%FBS.

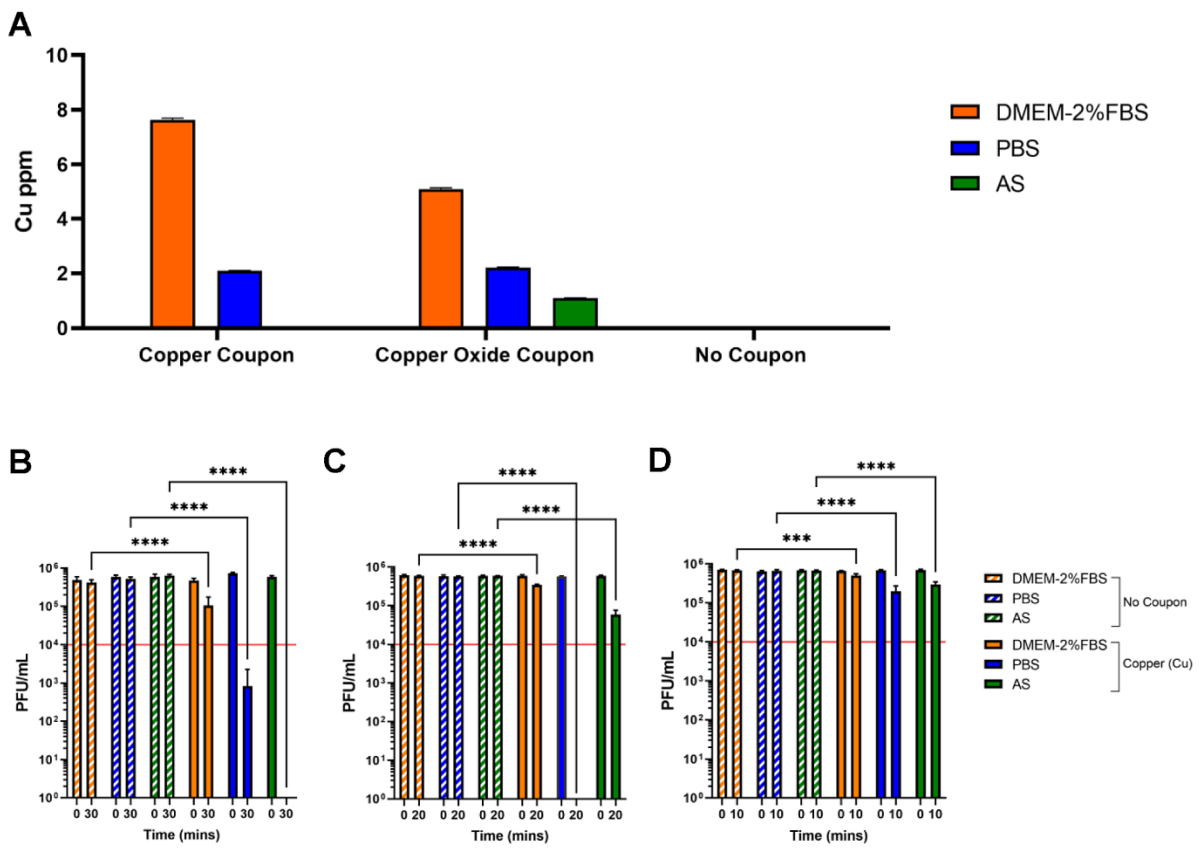

143

144

145 **FIG S7** Impact of different carrier solutions on copper ion dissolution and SARS-CoV-2
146 inactivation upon exposure to an evaporated copper thin-film surface. (A) ICP-OES
147 determined copper ion levels in DMEM-2%FBS, PBS or AS carrier solutions following 30-
148 min exposure to evaporated copper, Cu_2O thin film coupons or no coupon control. Data
149 shown represents mean values (n = 6 replicates and error bar = SD). (B-D) Titre of SARS-
150 CoV-2 (PFU/mL) resuspended in DMEM-2%FBS, PBS or AS carrier solutions and
151 exposed to evaporated copper surfaces for (B) 30, (C) 20 and (D) 10 min or the equivalent
152 no coupon control. Data shown represents mean values (n = 3 replicates and error bar =
153 SD). At the 30 min time point the data shown is representative of 3 independent
154 experiments, the 20- and 10-min time points were included in the 3rd and final

experimental repeat. Statistical significance was assessed using two-way ANOVA with Tukeys multiple comparison test, **** $p < 0.0001$, *** $p < 0.001$. The limit of detection (LOD) for the assay is indicated by the solid red line.

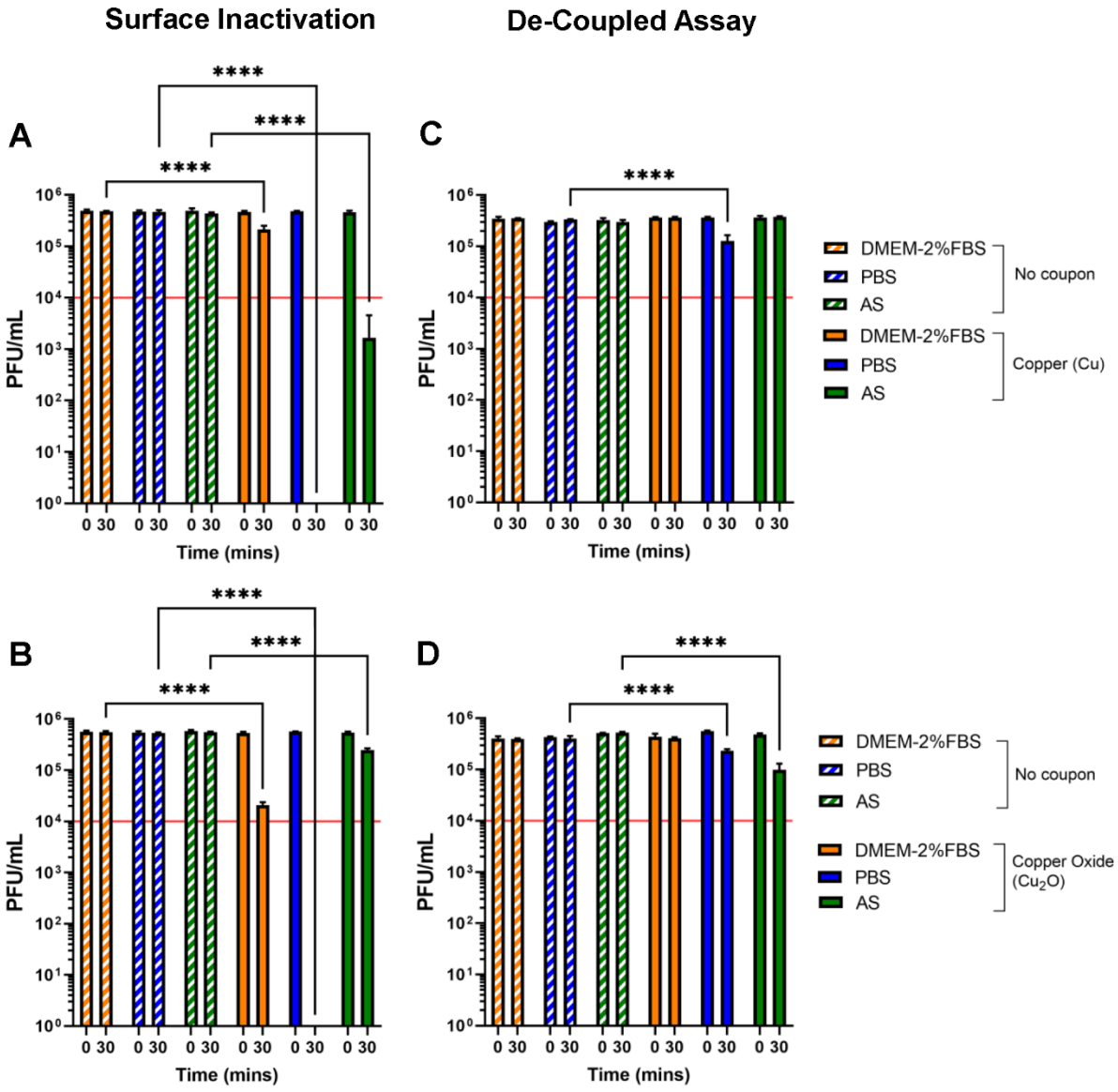

FIG S8 De-coupled ion dissolution SARS-CoV-2 inactivation assay. (A and B) test surface virus inactivation assay: Titre of SARS-CoV-2 (PFU/mL) resuspended in DMEM-2%FBS, PBS or AS carrier solutions and exposed to (A) evaporated copper or (B) Cu_2O thin-film

coupons for 0 or 30 minutes or the equivalent no coupon control. (C and D) de-coupled virus inactivation assay: carrier solution DMEM-2%FBS, PBS or AS exposed to evaporated copper (C) and Cu_2O (D) thin-film coupons for 0 or 30 min or the equivalent no coupon control. Following coupon exposure, the resultant solution is removed and spiked with SARS-CoV-2 and incubated for a further 0 or 30 min or the equivalent no coupon control. Data is shown as titre of SARS-CoV-2 (PFU/mL). Data represents mean values (n = 3 replicates and error bar = SD) and is representative of 3 independent experiments. Statistical significance was assessed using two-way ANOVA with Tukeys multiple comparison test, **** $p < 0.0001$. The limit of detection (LOD) for the assay is indicated by the solid red line.